DISSERTATIONES
PHYSICAE
UNIVERSITATIS
TARTUENSIS
123

SERGEY KOSHKAREV

A phenomenological feasibility study of the possible impact of the intrinsic heavy quark (charm) mechanism on the production of doubly heavy mesons and baryons

DISSERTATIONES PHYSICAE UNIVERSITATIS TARTUENSIS
123

DISSERTATIONES PHYSICAE UNIVERSITATIS TARTUENSIS
123

SERGEY KOSHKAREV

A phenomenological feasibility study of the possible impact of the intrinsic heavy quark (charm) mechanism on the production of doubly heavy mesons and baryons

UNIVERSITY OF TARTU
Press

Institute of Physics, University of Tartu, Estonia

Institute of Physics, Faculty of Science and Technology, University of Tartu. The dissertation was admitted on March 14th, 2020 in partial fulfillment of the requirements for the degree of Doctor of Philosophy in Physics, and was allowed for defense by the Council of the Institute of Physics, University of Tartu

Supervisor: Dr. Stefan Groote, University of Tartu

Opponents: Prof. Paul Hoyer, University of Helsinki, Helsinki, Finland
Prof. Boris Kopeliovich, Federico Santa Maria University, Valparaiso, Chile

Defense: May 14, 2020 at the University of Tartu

This work has been partially supported by the Graduate School of Functional Materials and Technologies at the University of Tartu, receiving funding from the European Regional Development Fund. In addition, the work of Sergey Koshkarev was supported in part by the European Regional Development Fund under Grant No. TK133 and by the Estonian Research Council under Grant No. PRG356.

ISSN 1406-0647
ISBN 978-9949-03-323-2 (print)
ISBN 978-9949-03-324-9 (pdf)

University of Tartu Press
www.tyk.ee

To the memory of my dearest friend Dr Alexander Rakitin

Contents

List of Figures

List of Tables

Acknowledgements

First of all, I am grateful to my family: Mom, Dad, Kseniia and Georgii. Thank you for everything.

I would like to thank my supervisor Stefan Groote for his constant support, help and patience. I would also like to thank Piret Kuusk, the retired head of the Laboratory of Theoretical Physics (LTP), for giving me the opportunity to join the LTP at the University of Tartu.

I am grateful to my co-authors: Vladimir Anikeev, Stanley J. Brodsky, Andrei Gridin, Stefan Groote and Alexey Guskov. It was a pleasure to collaborate with all of you, a collaboration which resulted in a number of papers we could publish together.

List of publications

The thesis is based on the following ten publications, the full texts of which are included at the end of the thesis.

I S. Koshkarev, V. Anikeev, Production of the doubly charmed baryons at the SELEX experiment – The double intrinsic charm approach,
Physics Letters B **765** (2017) 171

II S. Koshkarev, Production of the Doubly Heavy Baryons, B_c Meson and the All-charm Tetraquark at AFTER@LHC with Double Intrinsic Heavy Mechanism,
Acta Physica Polonica B **48** (2017) 163

III S. Koshkarev, S. Groote, Double quarkonium production at high Feynman-x,
Nuclear Physics B **915** (2017) 384

IV S. Groote, S. Koshkarev, Production of doubly charmed baryons nearly at rest,
The European Physical Journal C **77** (2017) 509

V S. J. Brodsky, S. Groote, S. Koshkarev, Resolving the SELEX–LHCb double-charm baryon conflict: the impact of intrinsic heavy-quark hadroproduction and supersymmetric light-front holographic QCD,
The European Physical Journal C **78** (2018) 483

VI S. Koshkarev, S. Groote, Signals of the double intrinsic heavy quark at the current experiments, Journal of Physics: Conference Series **938** (2017) 012054

VII S. Koshkarev, S. Groote, Resolving the SELEX–LHCb double-charm baryon conflict: the impact of intrinsic heavy-quark hadroproduction and supersymmetric light-front holographic QCD, EPJ Web of Conferences **204** (2019) 08007

VIII S. Koshkarev, Phenomenological analysis of the possible impact of Double Parton Scattering in double J/ψ production at the COMPASS detector using the CERN π^- beam at 190 GeV/c, arXiv:1909.06195 [hep-ph]

IX A. Gridin, S. Groote, A. Guskov, S. Koshkarev, Feasibility study for the search of intrinsic charm at the COMPASS experiment and at the STAR fixed-target program, arXiv:1901.01712 [hep-ph]

X S. Groote, S. Koshkarev, On the kinematic limit of the charm production in fixed-target experiments with the intrinsic charm from the target, arXiv:1901.04193 [hep-ph]

Approval of results

Results were discussed at the XVII Workshop on High Energy Spin Physics (September 11–15, 2017, Dubna, Russia), the XXIV International Baldin Seminar on High Energy Physics Problems "Relativistic Nuclear Physics and Quantum Chromodynamics" (September 17–22, 2018, Dubna, Russia), the XVIII Workshop on High Energy Spin Physics (September 2–6, 2019, Dubna, Russia), and at the COMPASS collaboration meetings (CERN). Results were also reported at the Doctor school conferences "Functional materials and technologies" in 2017, 2018 and 2019 (Tartu and Tallinn, Estonia) and at the student physics seminars (Tartu, Estonia).

Author's contribution

The author was the main contributor to almost all publications. In Ref. V the author contributed to the explanation of the production properties of the doubly charmed baryons, the review and the explanation of the experimental results and the preparation of the manuscript.

A remark about the structure of this thesis

After two introductory parts summarizing current experimental evidences for the existence of the intrinsic charm mechanism and providing the theoretical background, Chapters 3, 4,

5 and 6 contain the main results of the research and the summary. The appendices contain additional details.

This thesis is a compilation of the publications listed above. These publications are integral parts of the thesis and are attached to this thesis. However, besides connecting the different subjects, the text gives some extensions which are not contained in the publications.

1 Motivation

> "Begin at the beginning", the King said gravely, "and go on till you come to the end: then stop."
>
> Lewis Carroll,
> *Alice in Wonderland*

Almost four decades have passed since the intrinsic charm mechanism was proposed [1, 2], stating that heavy quarks are present in the proton's wavefunction from the outset.

The existence of heavy quarks in the proton's light-front (LF) wavefunction at a large LF momentum fraction x is in fact predicted by QCD if one analyzes the higher Fock states $|uudc\bar{c}\rangle$ and $|uudc\bar{c}c\bar{c}\rangle$ in the hadronic eigenstate, i.e., Fock states where the heavy quark pairs are multi-connected to the valence quarks[1]. LF wavefunctions, the eigensolutions of the QCD LF Hamiltonian, are defined at fixed LF time $\tau = t + z/c$ and are thus off-shell in the invariant mass. For example, in QED, positronium has an analogous Fock state $|e^+e^-\mu^+\mu^-\rangle$ due to the insertion of light-by-light scattering in the positronium self-energy amplitude. In such an "intrinsic charm" Fock state $|uudc\bar{c}\rangle$, the maximum kinematic configuration occurs at minimum invariant mass where all quarks are at rest in the hadron's rest frame, i.e., at equal rapidity in the moving hadron. Equal rapidity implies $x_i \propto (m^2 + \vec{k}_\perp^2)^{1/2}$ for each quark, so that the heavy quarks in the Fock state carry most of the hadron's LF momentum. Here $\vec{k}_\perp$ is the transverse momentum. The operator product expansion predicts that the probability of intrinsic heavy-quark Fock states $|uudQ\bar{Q}\rangle$ scales as $1/m_Q^2$ due to the non-Abelian couplings of QCD [3, 4].

Even though there is no clear observation of the mechanism, the baryonic states $\Lambda_c(udc)$ and $\Lambda_b(udb)$ were both discovered at the Intersecting Storage Rings (ISR) at CERN at high values of the Feynman momentum fraction x_F [5–7]. The SELEX experiment provided the observation of a double charm baryon $|ccd\rangle$ at a large mean value for x_F and a relatively

[1] At high values such an x is approximately equal to the Feynman-x which can be directly measured at experiments. Therefore, in this thesis we will use the symbol x_F.

small mean transverse momentum [8, 9]. In addition, the NA3 experiment measured both the single-quarkonium hadroproduction $\pi A \to J/\psi X$ [10] and the double-quarkonium hadroproduction $\pi A \to J/\psi J/\psi X$ [11] at high x_F. In fact, all of the $\pi A \to J/\psi J/\psi X$ events were observed with a total value of $x_F > 0.4$. Both the SELEX and the NA3 experiments provide unexpectedly high production rates.

This dissertation contains a phenomenological feasibility study of the production of the double charm baryons at high Feynman-x with the double intrinsic charm approach, aimed to resolve the apparent conflict between measurements of double-charm baryons by the SELEX fixed-target experiment and the LHCb experiment at the LHC collider. The observed spectroscopy of double-charm hadrons is in agreement with the predictions of supersymmetric light front holographic QCD. We also re-considered the associate quarkonium production at high Feynman-x and re-reviewed the NA3 results on the J/ψ pair production. Additionally, we analyzed the charm production from the fixed-target experiments with the intrinsic charm from the target.

2 Theoretical background: the BHPS model

> Of course the first thing to do was to make a grand survey of the country she was going to travel through. "It's something very like learning geography," thought Alice...
> "Principal rivers – there are none. Principal mountains – I'm on the only one, but I don't think it's got any name. What are those creatures, making honey down there? They can't be bees – nobody ever saw bees a mile off, you know -" and for some time she stood silent, watching one of them that was bustling about among the flowers, Insect spoking its proboscis into them, "just as if it was a regular bee," thought Alice.
> However, this was anything but a regular bee: in fact it was an elephant... "It'll never do to go down among them without a good long branch to brush them away..."
>
> Lewis Carroll,
> *Through the Looking-Glass*

The distribution of intrinsic heavy quarks is described by the BHPS model given by Brodsky, Hoyer, Peterson and Sakai [1, 2].

In the BHPS model the wavefunction of a hadron in QCD can be represented as a superposition of Fock state fluctuations, e.g. $|h\rangle \sim |h_l\rangle + |h_l g\rangle + |h_l Q\bar{Q}\rangle \ldots$, where h_l is the

light quark content, and $Q = c, b$. If the projectile interacts with the target, the coherence of the Fock components is broken and the fluctuation can hadronize. The intrinsic heavy quark Fock components are generated by virtual interactions such as $gg \to Q\bar{Q}$ where the gluons couple to two or more valence quarks of the projectile. The probability to produce such $Q\bar{Q}$ fluctuations scales as $\alpha_s^2(m_Q^2)/m_Q^2$ relative to the leading-twist production.

Following Refs. [1, 2, 12], the general formula for the probability distribution of an n-particle intrinsic heavy quark Fock state as a function of the momentum fractions x_i and the transverse momenta $\vec{k}_{T,i}$ can be written as

$$\frac{dP_{iQ}}{\prod_{i=1}^n dx_i d^2k_{T,i}} \propto \alpha_s^4(M_{Q\bar{Q}}) \frac{\delta\big(\sum_{i=1}^n \vec{k}_{T,i}\big)\delta\big(1-\sum_{i=1}^n x_i\big)}{\big(m_h^2 - \sum_{i=1}^n m_{T,i}^2/x_i\big)^2}, \tag{1}$$

where m_h is the mass of the initial hadron and $m_{T,i}^2 = m_i^2 + k_{T,i}^2$. The probability distribution for the production of two heavy quark pairs is given by

$$\frac{dP_{iQ_1Q_2}}{\prod_{i=1}^n dx_i d^2k_{T,i}} \propto \alpha_s^4(M_{Q_1\bar{Q}_1})\alpha_s^4(M_{Q_2\bar{Q}_2}) \frac{\delta\big(\sum_{i=1}^n \vec{k}_{T,i}\big)\delta\big(1-\sum_{i=1}^n x_i\big)}{\big(m_h^2 - \sum_{i=1}^n m_{T,i}^2/x_i\big)^2}. \tag{2}$$

If one is interested in the calculation of the x distribution, one can simplify the formula by replacing $m_{T,i}$ by the effective mass $\hat{m}_i = (m_i^2 + \langle k_{T,i}^2 \rangle)^{1/2}$ and neglecting the masses of the light quarks,

$$\frac{dP_{iQ_1Q_2}}{\prod_{i=1}^n dx_i} \propto \alpha_s^4(M_{Q_1\bar{Q}_1})\alpha_s^4(M_{Q_2\bar{Q}_2}) \frac{\delta\big(1-\sum_{i=1}^n x_i\big)}{\big(\sum_{i=1}^n \hat{m}_{T,i}^2/x_i\big)^2}. \tag{3}$$

The BHPS model assumes that the vertex function in the intrinsic heavy quark wavefunction is varying relatively slowly. The particle distributions are then controlled by the light-front energy denominator and the phase space. The Fock states can be materialized by a soft collision in the target which brings the state on shell. The distribution of produced open and hidden charm states will reflect the underlying shape of the Fock state wavefunction.

According to the intrinsic heavy quark mechanism the production cross sections $\sigma^{iQ}(Q\bar{Q})$ and σ^{iQQ} of a single and double $Q\bar{Q}$ pair production, respectively, is given by [12]

$$\sigma^{iQ}(Q\bar{Q}) = P_{iQ} \cdot \sigma^{inel} \cdot \frac{\mu^2}{4\hat{m}_Q^2}\,; \qquad \sigma^{iQQ}(Q\bar{Q}Q\bar{Q}) = \frac{P_{iQQ}}{P_{iQ}} \cdot \sigma^{iQ}, \tag{4}$$

where $\mu^2 \approx 0.2$ GeV denotes the soft interaction scale parameter and σ^{inel} is the inelastic cross section of hadron–hadron scattering.

It is interesting to note that in contrast to perturbative QCD (pQCD), in case of the intrinsic charm (IC) mechanism (extendable as intrinsic heavy quark mechanism for heavy quarks in general) the hadron–nucleus cross section will be

$$\sigma_{hN} = \sigma_{hp} \cdot A^{2/3}, \tag{5}$$

where σ_{hp} is the hadron–proton cross section (assumed to be approximately equal to the hadron–neutron cross section) and A is the nucleus mass in the atomic units.

3 Double quarkonium production at high Feynman-x

> He [Owl] had explained this to Pooh and Christopher Robin once before and had been waiting for a chance to do it again, because it is a thing you can easily explain twice before anybody knows what you are talking about.
>
> Alan Alexander Milne,
> *The House at Pooh Corner*

In the era of high luminosity and high energy accelerators the associate heavy quarkonium production plays a special role as a testing ground to study multiple parton scattering in a single hadron collision. Significant progress on the Double Parton Scattering (DPS) has been investigated by the Tevatron and the LHC by measuring the productions of $J/\psi + W$ [13], $J/\psi + Z$ [14], J/ψ+charm [15], and $J/\psi + J/\psi$ [16–20]. Therefore and for many other reasons, heavy quarkonium production is always a hot topic in high energy physics, as this kind of physics is an ideal probe for testing quantum chromodynamics.

In the early eightieth the NA3 collaboration provided low statistic result on the double J/ψ production at high Feynman-x [11].

Current colliders provide access only to the physics at low values of the Feynman parameter x_F. However, significant interest is given also for physics at high x_F [21–25]. This region will be accessible at a future fixed-target experiment at the LHC (AFTER@LHC).

In this chapter we discuss the impact of the double intrinsic heavy quark mechanism on the associate quarkonium production. We also re-review the double J/ψ production data provided by the NA3 experiment using the CERN π^- beam at 150 and 280 GeV/c with incident on a platinum target and finally provide predictions for the future AFTER@LHC program.

3.1 Double-quarkonium production cross section

The production cross section of the quarkonium can be obtained as an application of the quark–hadron duality principle [26]. In this model the cross section of quarkonium are obtained by calculating the production of a $Q\bar{Q}$ pair in the small invariant mass interval between $2m_Q$ and the threshold to produce open heavy-quark hadrons, $2m_H$. The $Q\bar{Q}$ pair has $3 \times \bar{3} = (1 + 8)$ color components, consisting of a color-singlet and a color-octet. Therefore, the probability that a color-singlet is formed and produces a quarkonium state is $1/(1 + 8)$, and the model predicts

$$\sigma(Q\bar{Q}) = \frac{1}{9}\int_{2m_Q}^{2m_H} dM_{Q\bar{Q}} \frac{d\sigma_{Q\bar{Q}}}{dM_{Q\bar{Q}}} = \frac{1}{9}\int_{4m_Q^2}^{4m_H^2} dM^2_{Q\bar{Q}} \frac{d\sigma_{Q\bar{Q}}}{dM^2_{Q\bar{Q}}}\,, \tag{6}$$

where $\sigma_{Q\bar{Q}}$ is the production cross section of the heavy quark pairs and $\sigma(Q\bar{Q})$ is a sum of production cross sections of all quarkonium states in the duality interval. For example, in case of charmonium states one has $\sigma(Q\bar{Q}) = \sigma(J/\psi) + \sigma(\psi(2S)) + \ldots$. According to a simple statistical counting, the fraction of the total color-singlet cross section into a quarkonium state is given by

$$\sigma(X) = \rho_X \cdot \sigma(Q\bar{Q}) \tag{7}$$

$(X = J/\psi, \psi(2S), \ldots)$ with

$$\rho_X = \frac{2J_X + 1}{\sum_i (2J_i + 1)}\,, \tag{8}$$

where J_X is the spin of the quarkonium state X and the sum runs over all quarkonium states. In case of the J/ψ meson the calculation gives

$$\rho_{J/\psi} \approx 0.2. \tag{9}$$

This statistical counting rule works well for J/ψ but not so well for other charmonium states, even not for $\psi(2S)$. In order to estimate cross sections for excited states, in this paper we use the fact that a quarkonium production matrix element is proportional to the absolute square of the radial wave function at the origin [27], so that

$$\sigma(J/\psi) : \sigma(\psi(2S)) \approx |R_{J/\psi}(0)|^2 : |R_{\psi(2S)}(0)|^2. \tag{10}$$

The absolute square of the radial wave function $R_X(0)$ of the quarkonium state $X = J/\psi, \psi(2S), \ldots$ at the origin is determined by the leptonic decay rate [28]

$$\Gamma(X \to e^+e^-) = \frac{4N_c\alpha_{\rm em}^2 e_Q^2}{3}\frac{|R_X(0)|^2}{M_X^2}\left(1 - \frac{16\alpha_s}{3\pi}\right), \tag{11}$$

where $N_c = 3$ is the number of quark colors, e_Q is the electric charge of the heavy quark, and M_X is the mass of the quarkonium state X. Splitting $\sigma(Q\bar{Q})$ up into the different quarkonium states one can obtain the corresponding production cross sections.

These formulas can be generalized for the calculation of the associate quarkonium production. For example, the double-quarkonium production cross section $\sigma(Q\bar{Q} + Q\bar{Q})$ from the Fock state $|uudQ\bar{Q}Q\bar{Q}\rangle$ can be written obviously as

$$\sigma^{iQQ}(Q\bar{Q} + Q\bar{Q}) = (f_{Q\bar{Q}/p}^{iQQ})^2\, P_{iQQ}\, \sigma_{pp}^{inel}\, \frac{1}{9}\frac{1}{9}\frac{\mu^2}{4\hat{m}_Q^2}, \tag{12}$$

where the fragmentation ratio $f_{Q\bar{Q}/p}^{iQ_1Q_2}$ is obtained as

$$f_{Q\bar{Q}/p}^{iQ_1Q_2} = \int_{4m_Q^2}^{4m_H^2} dM_{Q\bar{Q}}^2 \frac{dP_{iQ_1Q_2}}{dM_{Q\bar{Q}}^2} \Big/ \int_{4m_Q^2}^{s} dM_{Q\bar{Q}}^2 \frac{dP_{iQ_1Q_2}}{dM_{Q\bar{Q}}^2}. \tag{13}$$

The x_F distribution for the double quarkonium production $X_1 + X_2$ (with $X_i = J/\psi, \psi(2S), \Upsilon(1S), \Upsilon(2S), \ldots$) is then given by [12]

$$\begin{aligned}\frac{dP_{iQ_1Q_2}}{dx_{X_1X_2}} &= \int \prod_{i=1}^{n} dx_i dx_{X_1} dx_{X_2} \frac{dP_{iQ_1Q_2}}{\prod_{i=1}^n dx_i}\delta(x_{X_1X_2} - x_{X_1} - x_{X_2}) \\ &\quad \times\delta(x_{X_1} - x_{Q_1} - x_{\bar{Q}_1})\delta(x_{X_2} - x_{Q_2} - x_{\bar{Q}_2}).\end{aligned} \tag{14}$$

.

3.2 Revisiting the double J/ψ production at NA3

Using the CERN pion beam at 150 and 280 GeV/c to produce charm particles with incident on hydrogen and platinum targets, the NA3 experiment provided data on the production of the double J/ψ on platinum target in the kinematic region $x_F^*(J/\psi) > 0$ with the

respective production cross sections of $18 \pm 8\,\mathrm{pb}$ and $30 \pm 10\,\mathrm{pb}$ per nucleon and the ratio $\sigma(J/\psi J/\psi)/\sigma(J/\psi) = (3 \pm 1) \times 10^{-4}$ at both energies [2].

3.2.1 Acceptance of the NA3 detector

In order to understand the NA3 data, we give a short overview over the layout of the NA3 detector (see Ref. [29] for a more complete description). The NA3 detector consisted of a spectrometer with fixed targets of liquid hydrogen (proton target, 30 cm long) and platinum (nuclear target, 6 cm long). The targets were located at a distance of 45 cm.

For the measurements the NA3 experiment used the beams of p, $\bar{p}$, $K^{\pm}$, $\pi^{\pm}$ with intensities of $(3-5) \cdot 10^7$ particles per second. To reduce the particle flux through the spectrometer, a beam dump absorbing about 80% of the charged particle flux was installed behind the platinum target. The dump was made of a 1.5 m block of stainless steel and had a conical core made of tungsten and uranium. The aperture angle of the cone could be chosen as either 20 or 30 mrad. The stainless steel blocks surrounded the conical core of the dump. Along the beam behind the dump, other parts of the spectrometer were located such as a spectrometer magnet, tracking detectors, counter hodoscopes and trigger hodoscopes. At the end of the spectrometer an additional 1.8 m long iron absorber was placed which played the role of a muon filter and reduced the low energy particle background. Together with the other trigger hodoscopes, the trigger hodoscope placed behind the muon filter had the purpose to select muons originated from the targets. The trigger system imposed a condition on the vertical component of the transverse momentum of the muons. To be registered, a single muon had to satisfy the condition $p_T > 1\,\mathrm{GeV}/c$, while for two muons in the event one had to have $p_T > 0.6\,\mathrm{GeV}/c$ for each muon. Such requirements eliminated a large fraction of pion and kaon decays and rejected low mass resonances like ρ, ϕ and ω mesons.

In order to be registered, muons had to pass more than 3 m of iron. As charged particles, on this way they interacted with nucleons of the matter and spent some of their

[2] In this thesis x_F denotes the Feynman-x in the laboratory frame while x_F^* denotes the Feynman-x in the center-of-mass system.

energy for ionization and radiative effects. For example, by passing through 3 m of iron a muon with energy of 150 GeV looses more than 7.5 GeV of its energy. This leads to an acceptance notion which mostly depends on the geometry of the setup, but also on the kinematics of the particles.

In the data analysis for single J/ψ selection a criterium $x_F^* > 0$ was used for both the 150 GeV and 280 GeV data samples. For $x_F^* < 0$ the NA3 acceptance was dropping fast. This means that each of the J/ψ should have had a minimal longitudinal momentum to pass the setup and to be detected. For the 150 GeV beam this threshold in the laboratory system was about 27 GeV/c, and 39 GeV/c for the 280 GeV beam. For the double J/ψ state these thresholds should be multiplied roughly by two. Because the acceptance was dropping down near the threshold, there was a low probability to detect an event with a momentum close to the threshold. This means that it is not possible to detect a double J/ψ state with $x_F \sim 27/150$ for 150 GeV and with $x_F \sim 39/280$ for 280 GeV, i.e. $x_F < 0.4$ and $x_F < 0.3$ respectively, since low energy muons will either be absorbed by the matter of the setup or rejected by the trigger. In addition, because of the dropping of the acceptance, events detected *de facto* by NA3 have values of x_F larger than the thresholds for both data samples (cf. Fig. 1). The estimate for the NA3 setup acceptance for the double J/ψ production is done with a Monte Carlo approach using pairs of uncorrelated J/ψ's. It is definitely interesting to investigate the correctness of the acceptance obtained by such a Monte-Carlo simulation.

By investigating the kinematic distributions (cf. Fig. 2), one obtains a small difference in the momentum distribution between the J/ψ for the Single Parton Scattering (SPS) mechanism and a higher momentum gap for the uncorrelated J/ψ's sample. Such a gap in momentum and as the result of this also in the Feynman-x distributions could lead to the erroneous interpretation of the NA3 acceptance. Indeed, keeping in mind that the J/ψ pair has to carry a minimum x_F to be detected, a situation is possible where one of the J/ψ does not cary enough momentum to be triggered. Due to the larger momentum gap, the

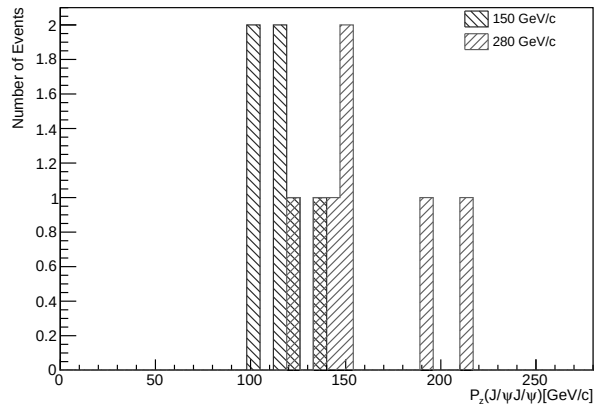

Figure 1: Momentum distributions of J/ψ pairs measured by the NA3 collaboration.

possibility of rejection can differ between SPS and the uncorrelated sample. Concluding the above discussion we can say that the cross section values provided by the NA3 might be not fully correct and the high Feynman-x region can be interpreted solely by the detector acceptance.

3.2.2 $\sigma(J/\psi J/\psi)$ production via Single Parton Scattering

Utilizing the fact that the double J/ψ production cross section can be normalized with a special choice of the composition $(\alpha_s f_\psi)^4$, where α_s is the strong coupling constant and f_ψ is the decay constant of J/ψ, in Ref. [33] it was found that most of the measured cross section is due to $q\bar{q} \to J/\psi J/\psi$. However, as mentioned above, such a high production rate is unexpected at NA3 energies. Therefore, instead of the double J/ψ production cross section it is interesting to analyze the production rate.

Using the NA3 rate it is easy to estimate that

$$\frac{\sigma(c\bar{c}+c\bar{c})}{\sigma(c\bar{c})} > 10^{-2}. \tag{15}$$

Even making the unrealistic assumption that all $c\bar{c}$ pairs in $\sigma(c\bar{c}+c\bar{c})$ are lying in the duality interval, the production rate seems to be absolutely untrusted.

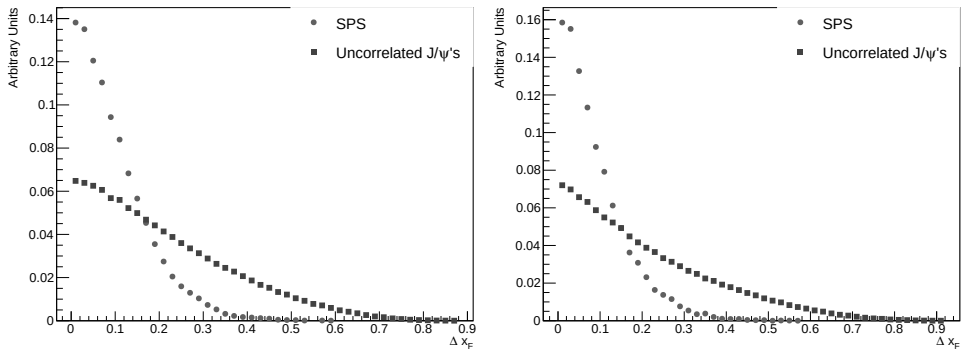

Figure 2: $\Delta x_F = |x_1(J/\psi) - x_2(J/\psi)|$ distributions for the uncorrelated J/ψ's and SPS production mechanisms at the 150 GeV/c (left panel) and at the 280 GeV/c π beam (right panel) at NA3. $x_1(J/\psi)$ and $x_2(J/\psi)$ denote the x_F for the first and the second J/ψ, respectively. The uncorrelated J/ψ's distribution is obtained using Pythia 8 [30], and the SPS distribution is obtained using HELAC-Onia [31, 32]. All distributions are normalized to unity.

3.2.3 $\sigma(J/\psi J/\psi)$ production via the Intrinsic Charm mechanism

The production of double J/ψ based on the intrinsic charm approach is discussed in detail in Refs. [12, 34]. Perturbative QCD and intrinsic charm contributions have principally different regions where the main statistic is expected (cf. Fig. 3). Based on this fact, in Ref. [12] it was assumed that all the NA3 data came from the intrinsic charm mechanism. However, as we have shown above this kinematic region is restricted due to the detector acceptance. Therefore, such an interpretation is too ambitious.

Concluding this chapter it is important to note that none of the discussed mechanisms, neither pQCD nor the intrinsic charm mechanism, can be interpreted as the sole production mechanism. In addition, it is not possible to determine the relative contribution, as both calculations, the pQCD calculation [33] as well as the calculation based on the intrinsic charm mechanism [12], are normalized to the NA3 data, assuming either of these to be the

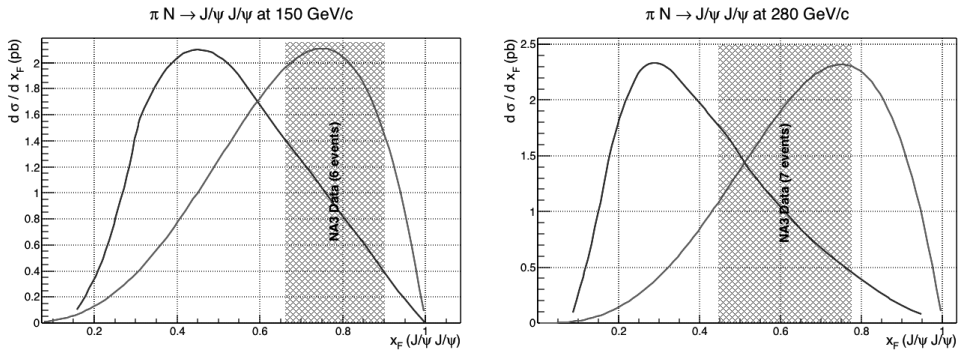

Figure 3: NA3 events (shaded area), pQCD prediction [33] (blue left curve) and prediction of the intrinsic charm mechanism (red right curve) at the 150 GeV/c (left panel) and at the 280 GeV/c π beam (right panel).

sole production mechanism.

3.3 Double J/ψ production at the COMPASS experiment

3.3.1 The COMPASS detector: short description

COMPASS, a fixed target experiment at CERN, uses the high intensity π^- beam of 190 GeV at the Super Proton Synchrotron at CERN for Drell–Yan (DY) measurements to produce charmonium, possible exotic states and dimuons in the set of polarized targets [35]. The experiment had several DY runs in 2014, 2015 and 2018.

The COMPASS DY configuration setup is quite similar to the NA3 setup. It uses two cylindrical cells (of 55 cm length and 4 cm in diameter each) of ammonia as a target and a hadron absorber to reduce the particle flux through the setup. The absorber made of alumina and stainless steel with the central tungsten plug is placed downstream of the target. The outgoing charged particles are detected by two spectrometers (Large Angle Spectrometer and Small Angle Spectrometer). At each spectrometer, the muon identification was accomplished by a system of muon filters. To be detected, at least two muon candidates from the target region should hit the trigger hodoscopes of the first

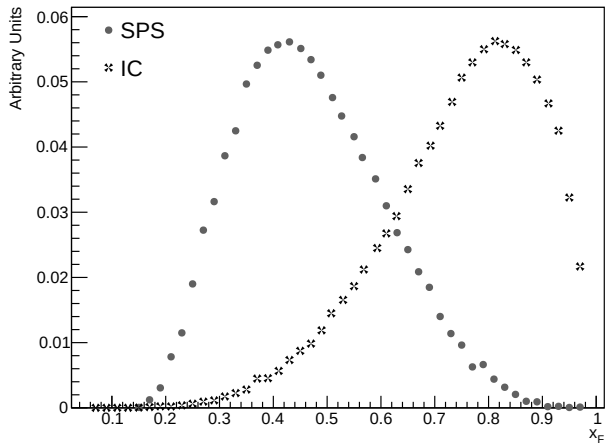

Figure 4: Prediction for the x_F distributions for SPS and the intrinsic charm production mechanisms at COMPASS. The SPS distribution is obtained by using HELAC-Onia [31,32], and the intrinsic charm distribution is obtained following Refs. [12]. All distributions are normalized to unity.

spectrometer ($25 < \theta_\mu < 160\,\text{mrad}$), or one should hit the trigger hodoscopes of the first and the other the trigger hodoscopes of the second spectrometer ($8 < \theta_\mu < 45\,\text{mrad}$). A muon passed through the peripheral part of the absorber and the material of one of two muon filters (stainless steel or concrete) loses an energy of about 10 GeV, defining the lower limit for its reconstruction.

3.3.2 Double J/ψ production at COMPASS

As COMPASS has a similar detector setup as the one at NA3, we can estimate that double J/ψ events detected by COMPASS should have $x_F > 0.3$ as threshold. Therefore, COMPASS can give a significant contribution to the understanding of the double J/ψ production mechanisms. In 2015 the COMPASS collaboration collected about one million

of dimuon events in the NH_3 target [36], and a factor of at least 1.5 more statistics is expected in the 2018 run [37]. Comparing the J/ψ statistics collected by NA3 [10] and the acceptance of the COMPASS detector one can estimate up to 100 double J/ψ events for the COMPASS experiment.

Taking into account that perturbative QCD and intrinsic charm contributions have principally different slopes and different regions for the main statistics to be expected, we propose to use x_F for the search for signals of the intrinsic charm mechanism and the determination of the relative contribution. The x_F distribution for the COMPASS kinematics and for the different production mechanisms are shown in Fig. 4.

As we already mentioned above, it is not possible to predict the relative contribution of the mechanism. However, it is interesting to estimate upper limits for both SPS and IC mechanisms.

3.3.3 Single Parton Scattering

Following calculations of the double J/ψ production cross section in SPS from Ref. [38] we can find a ratio between the double J/ψ production cross sections with a π^- beam at NA3 and COMPASS energies:

$$\sigma_{J/\psi J/\psi}(150\,\mathrm{GeV}/c) : \sigma_{J/\psi J/\psi}(190\,\mathrm{GeV}/c) : \sigma_{J/\psi J/\psi}(280\,\mathrm{GeV}/c) \approx 1 : 2.06 : 3.34\,. \quad (16)$$

Using the mean values for the double J/ψ production cross sections measured by NA3 of $18 \pm 8\,\mathrm{pb}$ and $30 \pm 10\,\mathrm{pb}$ per nucleon at 150 and $280\,\mathrm{GeV}/c$ as reference points, we find $\sigma(J/\psi J/\psi) \approx (12 - 29)\,\mathrm{pb}$ per nucleon at $190\,\mathrm{GeV}/c$ (cf. Fig. 5).

3.3.4 Intrinsic Charm

Following Ref. [12], we cast the double J/ψ production cross section into the form

$$\sigma_{J/\psi J/\psi} = f^2_{\psi/\pi} \frac{P_{icc}}{P_{ic}} \sigma_{ic}, \quad (17)$$

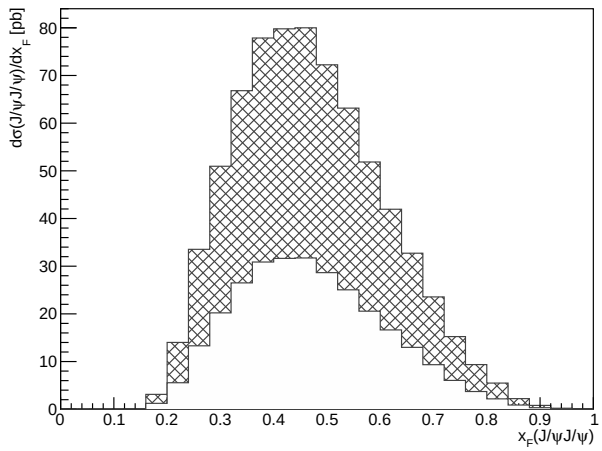

Figure 5: Prediction for the x_F distributions for SPS at COMPASS. The shape of the SPS distribution is obtained by using HELAC-Onia [31, 32]. The region $x_F < 0.3$ is excluded by the COMPASS acceptance.

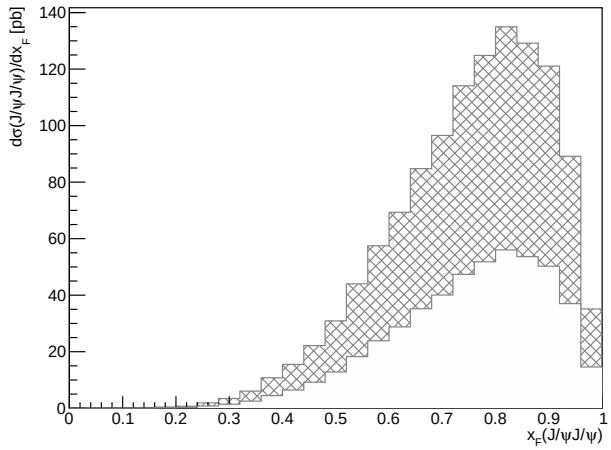

Figure 6: Prediction for the x_F distributions for the IC mechanism at COMPASS. The region $x_F < 0.3$ is excluded by COMPASS acceptance.

where $f_{\psi/\pi} \approx 0.03$ is the fraction of $c\bar{c}$ quark pairs producing J/ψ, P_{ic} and P_{icc} are probabilities to produce intrinsic $c\bar{c}$ and $c\bar{c}c\bar{c}$ Fock states, respectively, and $\sigma_{ic} \approx 0.5\,\mu$b is the intrinsic charm cross section for a π^- beam momentum of $200\,\text{GeV}/c$. Assuming P_{icc} to be independent of the projectile, the value $P_{icc} = 4.4\%P_{ic}$ was found in Ref. [12], and assuming $\sigma(J/\psi J/\psi)/\sigma(J/\psi)$ to be independent of the projectile, $P_{icc} = 10.6\%P_{ic}$ was found in the same Ref. [12]. Using these values, it is easy to estimate the double J/ψ production cross section at the COMPASS energy to be $(19.8 - 47.7)\,\text{pb}$ per nucleon (cf. Fig. 6).

3.3.5 Double Parton Scattering

Even though we don't expect DPS to be the leading production mechanism at the COMPASS energy ($\sqrt{s} \approx 19\,\text{GeV}$), this contribution is expected to be far from zero (cf. the lower panel in Fig. 7) [39].

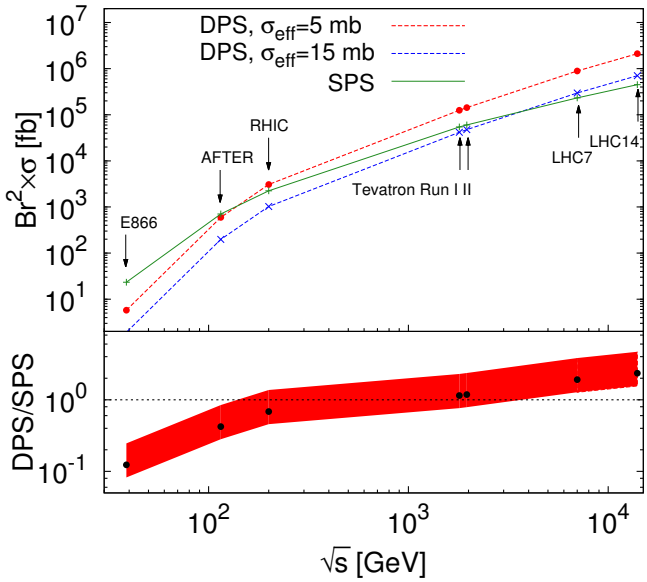

Figure 7: (Upper panel) Cross sections of (prompt-)J/ψ pair production via SPS and DPS mechanisms for two values of $\sigma_{\rm eff}$ as a function of $\sqrt{s}$. (Lower panel) DPS over SPS yield ratio for $5 < \sigma_{\rm eff} < 15\,$mb. The black circles correspond to 10 mb. Aside from the choice of $\sigma_{\rm eff}$, no theoretical uncertainties are included [39].

In case of hadron–nucleus collisions the general formula for the predicted DPS cross section for J/ψ pairs is given by [40]

$$\sigma^{hA}_{\rm DPS}(J/\psi J/\psi) = \frac{1}{2}\frac{\sigma(J/\psi)^{hN}\sigma(J/\psi)^{hN}}{\sigma^{hA}_{\rm eff}}\,, \tag{18}$$

where $\sigma(J/\psi)^{hN}$ denotes the single J/ψ hadron–nucleon cross section and $\sigma^{hA}_{\rm eff}$ is the effective hadron–nucleus DPS cross section.

Let us remind the reader that in Eq. (18) the production of each J/ψ in hadron–nucleon collisions is assumed to be an independent process. However, it is easy to see that the production threshold of the J/ψ pair is already more than 30% of the COMPASS energy (cf. Tab. 1). Therefore, we cannot assume the production of charmonium states as independent processes.

Table 1: Energy scales for Super Proton Synchrotron, Tevatron and LHC accelerators

Accelerator	Energy ($\sqrt{s}$)	Colliding Mode
Super Proton Synchrotron	$\sim 19\,\text{GeV}$	π^--Nucleus
Tevatron	$1.96\,\text{TeV}$	$\bar{p}p$
LHC	$7-14\,\text{TeV}$	pp

In order to estimate the kinematic suppression at the COMPASS energy we investigate the difference in the production of the single J/ψ in SPS and DPS (cf. Fig. 8).

As we can see, the J/ψ's from DPS are suppressed relatively to the J/ψ's from SPS. We can estimate the kinematic suppression factor as $\aleph \sim 0.7$. Accordingly, Eq. (18) can be cast into the form

$$\sigma^{\pi^- A}_{\rm DPS}(J/\psi J/\psi) = \frac{\aleph^2}{2}\frac{\sigma(J/\psi)^{\pi^- N}\sigma(J/\psi)^{\pi^- N}}{\sigma^{\pi^- A}_{\rm eff}}\,. \tag{19}$$

Utilizing the π^- beam at $200\,\text{GeV}/c$ with incident on hydrogen and platinum targets, the NA3 experiment provided a single J/ψ cross section in the $x^*_F > 0$ kinematic region,

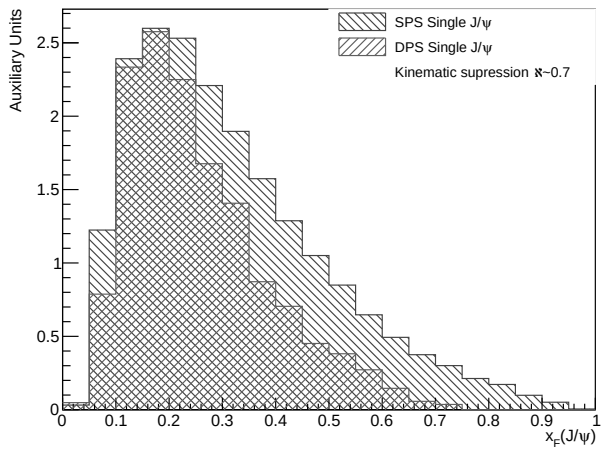

Figure 8: Feynman-x distribution of the production production cross section of the single J/ψ as independent process, i.e. SPS and the respective distribution in case of DPS, at COMPASS. Both distributions are obtained by using Pythia 8 [30].

$\sigma(J/\psi) \times Br(J/\psi \to \mu^+\mu^-) = 6.3 \pm 0.9\,\text{nb}$ and $\sigma(J/\psi) \times Br(J/\psi \to \mu^+\mu^-) = 960 \pm 150\,\text{nb}$ per nucleus for hydrogen and platinum, respectively [10]. For a heavy nucleus like platinum or tungsten, $\sigma_{\text{eff}}^{\pi^- A}$ is parametrized as [40]

$$\frac{\sigma_{\text{eff}}^{\pi^- N}}{\sigma_{\text{eff}}^{\pi^- A}} \approx 3A\,(\sim 600). \tag{20}$$

The value of $\sigma_{\text{eff}}^{\pi^- N}$ is unknown. The value of $\sigma_{\text{eff}}^{pp} \approx 5\,\text{mb}$ is measured in double J/ψ production (cf. Tab. 2) and $\sigma_{\text{eff}}^{\pi\pi} = 41\,\text{mb}$ is calculated [41]. Comparing these values, we see that in the pion–pion case the value of σ_{eff} is higher. Therefore, we can choose $\sigma_{\text{eff}}^{pp} \approx 5\,\text{mb}$ to obtain the upper limit

$$\sigma_{\text{DPS}}^{\pi^- N}(J/\psi J/\psi) \lesssim 1\,\text{pb/nucleon}. \tag{21}$$

Table 2: σ_{eff} extracted from double J/ψ production data.

Experiment	Energy	Colliding Mode	σ_{eff} (mb)
DØ [17]	1.96 TeV	$p\bar{p}$	4.8 ± 2.5
ATLAS [20]	8 TeV	pp	6.3 ± 1.9
LHCb [19]	13 TeV	pp	$8.8 - 12.5$

3.4 Associate quarkonium production at high Feynman-x at the AFTER@LHC

AFTER@LHC is the scheduled future fixed-target experiment at the LHC operating at $\sqrt{s} = 115\,\text{GeV}$. It is definitely interesting to estimate the associate quarkonium production.

Formula (12) still has one undefined parameter, the cross section σ_{pp}^{inel} for inelastic proton–proton scattering. In the region of $\sqrt{s} \geq 100$ GeV is obtained by the approximation [42]

$$\sigma_{pp}^{inel} = \left(62.59\,\hat{s}^{-0.5} + 24.09 + 0.1604\,\ln(\hat{s}) + 0.1433\,\ln^2(\hat{s})\right)\,\text{mb}, \tag{22}$$

where $\hat{s} = s/2m_p^2$. At the AFTER@LHC energy $\sqrt{s} = 115$ GeV, one obtains $\sigma_{pp}^{inel} \approx 37\,\text{mb}$.

3.4.1 Double-charmonium production from $|uudc\bar{c}c\bar{c}\rangle$

Combining Eqs. (12) and (13), we use $m_c \approx 1.3$ GeV for the mass of c quark, $\hat{m}_c = 1.5$ GeV for the effective transverse c-quark mass, and $m_D = 1.87$ GeV for the mass of the D meson. For the integrated probability distribution we take the value $P_{icc} \simeq 0.002$ [12]. For $Q = c$ and $H = D$ we may expect the double-charmonium production cross section to be

$$\sigma^{icc}(c\bar{c} + c\bar{c}) \approx 2.0 \times 10^2\,\text{pb}.$$

Analyzing the values of the radial wave functions at the origin [28], one finds

$$\sigma(J/\psi + J/\psi) : \sigma(J/\psi + \psi(2S)) : \sigma(\psi(2S) + \psi(2S)) \approx 1 : 0.65 : 0.43$$

Taking into account Eq. (9) and the generalization of Eq. (7),

$$\sigma(X_1 + X_2) = \rho_{X_1}\rho_{X_2} \cdot \sigma(Q\bar{Q} + Q\bar{Q}), \tag{23}$$

one obtains

$$\begin{aligned}
\sigma^{icc}(J/\psi + J/\psi) &\approx 7.8\,\text{pb} \\
\sigma^{icc}(J/\psi + \psi(2S)) &\approx 5.1\,\text{pb} \\
\sigma^{icc}(\psi(2S) + \psi(2S)) &\approx 3.4\,\text{pb}
\end{aligned} \tag{24}$$

3.4.2 Associated charmonium–bottomonium production from $|uudc\bar{c}b\bar{b}\rangle$

Following Refs. [12,43], the associated charmonium–bottomonium production cross section is given by

$$\sigma^{icb}(c\bar{c} + b\bar{b}) = f_{c\bar{c}/p}^{icb}\, f_{b\bar{b}/p}^{icb}\, P_{icb}\, \sigma_{pp}^{incl} \frac{1}{9}\frac{1}{9}\frac{\mu^2}{4\hat{m}_b^2}\left(\frac{\hat{m}_c}{\hat{m}_b}\frac{\alpha_s(M_{b\bar{b}})}{\alpha_s(M_{c\bar{c}})}\right)^4. \tag{25}$$

Applying Eq. (13) to this case ($Q = b$, $H = B$) we use $m_b \approx 4.2$ GeV for the mass of the b quark, $\hat{m}_b = 4.6$ GeV for the effective transverse b-quark mass, and $m_B = 5.3$ GeV for the mass of the B meson. The value of P_{icb} is unknown at this moment but we assume

it to be approximately equal to P_{icc}. Finally, we calculate the associated charmonium–bottomonium production cross section to be

$$\sigma^{icb}(c\bar{c} + b\bar{b}) = 0.46\,\text{pb}. \tag{26}$$

Here we calculate only the production cross section for the ground states,

$$\sigma^{icb}(J/\psi + \Upsilon(1S)) \approx 18\,\text{fb}. \tag{27}$$

3.4.3 Double-bottomonium production from $|uudb\bar{b}b\bar{b}\rangle$

We already have all ingredients for the calculation of the production cross section of the double-bottomonium states except for $P_{ibb} = (\hat{m}_c/\hat{m}_b)^2 \cdot P_{icb}$, so the numerical value will be

$$\sigma^{ibb}(b\bar{b} + b\bar{b}) = 0.04\,\text{pb}, \tag{28}$$

and the cross sections for the particular double-botomonium states are given by

$$\begin{aligned}
\sigma^{ibb}(\Upsilon(1S) + \Upsilon(1S)) &\approx 1.6\,\text{fb} \\
\sigma^{ibb}(\Upsilon(1S) + \Upsilon(2S)) &\approx 0.8\,\text{fb} \\
\sigma^{ibb}(\Upsilon(2S) + \Upsilon(2S)) &\approx 0.4\,\text{fb}
\end{aligned} \tag{29}$$

4 Resolving the SELEX–LHCb double-charm baryon conflict: the impact of intrinsic heavy-quark hadroproduction and supersymmetric light-front holographic QCD

> "I can't believe that!" said Alice.
>
> "Can't you?" the Queen said in a pitying tone. "Try again: draw a long breath, and shut your eyes."
>
> Alice laughed. "There's not use trying," she said: "one can't believe impossible things."
>
> "I daresay you haven't had much practice," said the Queen. "When I was your age, I always did it for half-an-hour a day. Why, sometimes I've believed as many as six impossible things before breakfast!"
>
> Lewis Carroll,
>
> *Through the Looking-Glass*

The first experimental evidence for the existence of double-charm baryons was published by the SELEX collaboration 15 years ago [8, 9, 44–47]. By utilizing the Fermilab negative and positive charged beams at $600\,\mathrm{GeV}/c$ to produce charmed particles in a thin foil of copper or on a diamond target, the SELEX collaboration observed two different decay channels for the $|dcc\rangle$ state at a mass close to $3520\,\mathrm{MeV}/c^2$.

The SELEX fixed-target experiment measured hadron production in the forward kinematic domain $x_F > 0.1$. The negative beam composition was about 50% Σ^- and 50% π^-, whereas the positive beams were composed of 90% protons. The experimental data

recorded used both positive and negative beams: 67% of the events were induced by Σ^-, 13% by π^-, and 18% by protons. In the first observation using the sample of $\Lambda_c^+ \to pK^-\pi^+$ [48, 49] SELEX found a signal of 15.9 events over 6.1 ± 0.1 background events in the channel $\Xi_{cc}^+ \to \Lambda_c^+ K^-\pi^+$ [8]. To complement this result, SELEX published an observation of 5.62 signal events over 1.38 ± 0.13 background events for the decay mode $\Xi_{cc}^+ \to pDK^-$ from a sample of $D^+ \to K^-\pi^+\pi^+$ decays [9]. The SELEX measurements imply that the lifetime of Ξ_{cc}^+ is less than 33 fs at 90% confidence level. The large $\langle x_F \rangle \sim 0.33$ and small $\langle p_T \rangle \approx 1\,\mathrm{GeV}/c$ are not amenable to perturbative QCD analysis.

Recently, the LHCb collaboration published an observation of 313 ± 33 events of $\Xi_{cc}^{++} \to \Lambda_c^+ K^-\pi^+\pi^+$ in a 13 TeV sample at the LHC and 113 ± 21 events in a 8 TeV sample at mass $3621.40 \pm 0.72(\mathrm{stat}) \pm 0.27(\mathrm{sys}) \pm 0.14(\Lambda_c^+)\,\mathrm{MeV}/c^2$, corresponding to $1.7\,\mathrm{fb}^{-1}$ and $2\,\mathrm{fb}^{-1}$, respectively [50]. The lifetime was measured to be $256^{+24}_{-22}(\mathrm{stat}) \pm 14(\mathrm{sys})$ fs [51]. Using the data sample corresponds to an integrated luminosity of $1.7\,\mathrm{fb}^{-1}$ at 13 TeV the LHCb confirmed the previous result with observation of $\Xi_{cc}^{++} \to \Xi_c^+\pi^+$ decay with signal yield is 91 ± 20 and the mass value is $3620.6 \pm 1.5(\mathrm{stat}) \pm 0.4(\mathrm{sys}) \pm 0.3(\Xi_c^+)\,\mathrm{MeV}/c^2$ [52].

LHCb reported that the mass difference between the $\Xi_{cc}^+(dcc)$ candidate reported by SELEX and the $\Xi_{cc}^{++}(ucc)$ state reported by LHCb was $103\,\mathrm{MeV}/c^2$, so these states cannot be readily interpreted as an isospin doublet since one would expect a mass difference of isospin partners to differ by only a few MeV/c^2.

It should be emphasized that SELEX observed the weak decay of the 3520 MeV double-charm baryon in two different decay channels, namely $\Xi_{cc}^+(3519 \pm 1) \to \Lambda_c^+ K^-\pi^+$ and $\Xi_{cc}^+(3518 \pm 3) \to pD^+\pi^-$ with statistical significances of 6.3 σ and 4.8 σ, respectively. The probability that these two signals are statistical fluctuations is extremely small.

In this chapter we show that the intrinsic heavy-quark QCD mechanism for the hadroproduction of heavy hadrons at large x_F can resolve the apparent conflict between measurements of double-charm baryons by the SELEX fixed-target experiment and the LHCb experiment at the LHC collider. We show that in fact both experiments are compatible, and that both can be correct. The observed spectroscopy of double-charm hadrons is in agreement with the predictions of supersymmetric light front holographic QCD.

4.1 Production rate and the kinematics of the Ξ_{cc}^+ for the SELEX experiment

The production cross section for the double charm baryon state $|dcc\rangle$ was not provided by the SELEX collaboration. However, the production properties of the doubly charmed baryons can be compared to that of the Λ_c^+ baryon. The production ratio $R_{\Lambda_c^+}$ measured by SELEX is given by

$$R_{\Lambda_c^+}^{\rm SELEX} = \frac{\sigma(\Xi_{cc}^+) \cdot Br(\Xi_{cc}^+ \to \Lambda_c^+ K^- \pi^+)}{\sigma(\Lambda_c^+)} = \frac{N_{\Xi_{cc}^+}}{\epsilon_+} \cdot \frac{\epsilon_{\Lambda_c^+}}{N_{\Lambda_c^+}},$$

where N is the number of events in the respective sample, and the reconstruction efficiency of Ξ_{cc}^+ is given by $\epsilon_+ \approx 11\%$ [8]. The central value for the number $N_{\Lambda_c^+}/\epsilon_{\Lambda_c^+}$ of reconstructed Λ_c^+ baryon events reported in Ref. [53] lies between 13326 and 10010 according to whether the lowest bin with $x_F \in [0.125, 0.175]$ is taken into account or not (cf. Appendix A). Therefore, we obtain

$$R_{\Lambda_c^+}^{\rm SELEX} \approx 0.012 - 0.014.$$

If we take into account the intrinsic charm mechanism, the reconstruction efficiency of Ξ_{cc}^+ will grow at least by a factor of 2.3, mainly because the x_F distribution predicted by the intrinsic charm mechanism at large Feynman x_F is well matched to the acceptance of the SELEX fixed-target experiment (see Fig. 9 for the acceptance for perturbative QCD and intrinsic charm). As a consequence, $R_{\Lambda_c^+}^{\rm SELEX}$ can be even smaller, about $(0.5 - 0.6) \times 10^{-3}$. This result is obviously higher than the ratio of the di-charm quark production cross section to the charm cross section, about $10^{-6} - 10^{-5}$ [54] predicted by perturbative QCD.

It is clearly of interest to relate the production of the Ξ_{cc}^+ at the SELEX experiment with the production of double J/ψ production at the NA3 experiment. Unfortunately, it is not possible to compare the two results directly. However, we are able to compare the following ratios $R = \sigma(c\bar{c}c\bar{c})/\sigma(c\bar{c})$:

$$R^{\rm SELEX} = R_{\Lambda_c^+} \times \frac{f(c \to \Lambda_c^+)}{f_{\Xi_{cc}}} \sim (1 - 4) \times 10^{-3}$$

and

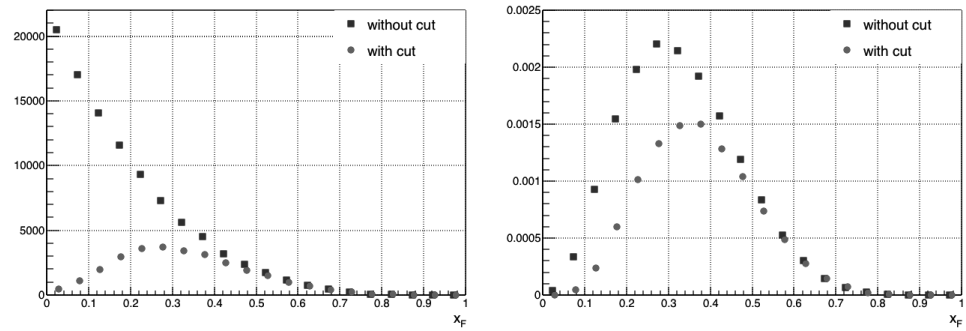

Figure 9: The squared (blue) points represent theoretically motivated distributions and the circular (red) points show this distribution with the experimental geometry cut. The pQCD motivated x_F distribution of Ξ_{cc}^{++} baryons [44] (left panel). The IC motivated x_F distribution of Ξ_{cc}^{++} baryons (right panel).

$$R^{\rm NA3} = \frac{\sigma(\psi\psi)}{\sigma(\psi)} \times \frac{f_\psi}{f_{\psi/\pi}^2} \sim 2 \times 10^{-2},$$

where $f_{\psi/\pi} \approx 0.03$ is the fragmentation rate of the intrinsic charm state of the pion into J/ψ [12] and $f_\psi \approx 0.06$ is the perturbative QCD fragmentation rate into J/ψ [55]. Using formula (13) we find $f_{\Xi_{cc}} \approx 0.25$ which represents the fraction of double $c\bar{c}$ pairs producing the sum of single-charged baryons Ξ_{cc}^{+} and double-charged baryons Ξ_{cc}^{++}, but this fraction cannot be less than the fraction to produce J/ψ. Therefore, $R^{\rm SELEX}$ should not be larger than 10^{-2}. The SELEX production ratio is thus in approximate consistency with the complementary measurement of the double J/ψ production by the NA3 experiment. Using formula (14) it is interesting to estimate that the intrinsic charm mechanism predicts $\langle x_F(\Xi_{cc})\rangle = 0.33$. This is in excellent agreement with the value $\langle x_F(\Xi_{cc}^{+})\rangle \sim 0.33$ measured by the SELEX experiment.

4.2 Mass difference

In order to resolve the discrepancy between the results from SELEX and LHCb we will utilize the predictions of the supersymmetric light front holographic QCD (SUSY LFHQCD).

This approach was developed by imposing the constraints from the superconformal algebraic structure on LFHQCD for massless quarks [56]. As has been shown in Refs. [56, 57], supersymmetry holds to a good approximation, even if conformal symmetry is strongly broken by the heavy quark mass.

Note that the $3_C + \bar{3}_C$ diquark structure of the Ξ_{cc}^+ can be written explicitly as $|[dc]c\rangle$ state.[3] The production of the double-charm baryon $\Xi_{[dc]c}^+$ with $[dc]$ in a spin-singlet state is natural in the SELEX fixed target experiment since it has acceptance at high x_F, i.e., in the realm of intrinsic charm; the $[dc]c$ configuration can easily re-coalesce from a higher Fock state of the proton such as $|uudc\bar{c}c\bar{c}\rangle$. In contrast, the production of this state is likely to be suppressed in $q\bar{q} \to c\bar{c}c\bar{c}$ or $gg \to c\bar{c}c\bar{c}$ reactions at the LHCb. Thus LHCb has most likely observed the double-charm baryon state $|u(cc)\rangle$, as will be explained in the next section. The mass difference between the $|[dc]c\rangle$ and the $|u(cc)\rangle$ states is due to the hyperfine interaction between the quarks.

Supersymmetric light front holographic QCD, if extended to the case of two heavy quarks, predicts that the mass of the spin-1/2 baryon should be the same as the mass of $h_c(1P)(3525)$ meson [57]. This is well compatible with the SELEX measurement of $3520.2 \pm 0.7\,\mathrm{MeV}/c^2$ for the $\Xi_{cc}^+(d[cc])$, although the uncertainty of SUSY LFHQCD predictions is at least of the order of 100 MeV. Indeed, the mass of the $|u(cc)\rangle$ state is predicted to be the same as that of the $\chi_{c2}(1P)(3556)$ meson, which is in turn lower than the LHCb result of $3621.40 \pm 0.72(\mathrm{stat}) \pm 0.27(\mathrm{sys}) \pm 0.14(\Lambda_c^+)\,\mathrm{MeV}/c^2$ for the Ξ_{cc}^{++}.

Supersymmetric LFHQCD is based on and best tested in the chiral limit of QCD, where all quarks are massless. The mass difference between the $h_c(1P)$ and the $\chi_{c2}(1P)$ is mainly due to the hyperfine splitting between the two charm quarks, and hence very small. In the baryon there is also the larger spin–spin interaction between the c and a light quark. By comparing hadron masses with light and charmed quarks, one can estimate the strength of this additional, the supersymmetry-breaking interaction in the range $84 - 136\,\mathrm{MeV}/c^2$ [57, 58], which is well compatible with the mass difference between

[3] We use square brackets [ ] for spin-0 and round brackets ( ) for spin-1 internal states.

the SELEX and the LHCb states.

4.3 The SELEX state at the LHCb

In the previous section we identified the SELEX state as a $|[dc]c\rangle$ state and the LHCb state as a $|u(cc)\rangle$ state of the double charmed baryon. While the SELEX state is definitely a spin-1/2 state, both $J^P = 1/2^+$ and $J^P = 3/2^+$ are possible assignments for the LHCb state. As becomes clear in the following, $J^P = 1/2$ is favored by the LHCb mass measurement and the very suppressed radiative decay to $|[qc]c\rangle + \gamma$. Based on the Heavy Quark Effective Theory (HQET), in Ref. [59] the baryon masses are estimated to be $3610\,\mathrm{MeV}/c^2$ for the spin-1/2 state $|u(cc)\rangle_{1/2^+}$ and $3680\,\mathrm{MeV}/c^2$ for the spin-3/2 state $|u(cc)\rangle_{3/2^+}$. For a qualitative estimate one can also compare with the nucleon states where the lowest mass $I = 1/2$, $J^P = 3/2^+$ state is $N(1720)$ which is considerably more massive than the proton.

It is interesting to analyze the ability of the LHCb experiment to observe the $|dcc\rangle$ state, i.e. Ξ_{cc}^+. Note that in a sample corresponding to $0.65\,\mathrm{fb}^{-1}$ of integrated luminosity at 7 TeV, in case of the decay process $\Xi_{cc}^+ \to \Lambda_c^+ K^- \pi^+$ the LHCb collaboration published an upper limit for the ratio $\sigma(\Xi_{cc}^+) \cdot Br(\Xi_{cc}^+ \to \Lambda_c^+ K^- \pi^+)/\sigma(\Lambda_c^+)$ of 1.5×10^{-2} and 3.9×10^{-4} for the lifetimes 100 fs and 400 fs, respectively [60]. Using the Ξ_{cc}^{++} lifetime recently measured by LHCb [51] we can estimate that the lifetime of Ξ_{cc}^+ is less then 100 fs (cf. the discussion in Section 4.5). Therefore, the LHCb provided an analysis which was outside the signal region for Ξ_{cc}^+.

It is also of interest to analyze the expectation of the production ratio between states. As we discussed above, the production of the double-charm baryons at the LHCb is due to the reactions $q\bar{q} \to c\bar{c}c\bar{c}$ or $gg \to c\bar{c}c\bar{c}$ with the following fragmentation of the cc-diquark into the double-charm baryons. Due to the Pauli principle the cc-diquark has to be a state with spin 1 or higher, leading to a state $|q(cc)\rangle$ with higher mass. The normalization of the fragmentation of the cc-diquark into the double-charm baryons is unknown. However, we are still able to provide some quantitative analysis. The fragmentation function is proportional to the wave function at the origin. The color-anti-triplet wave function can

be estimated on the basis of information about the color-singlet wave function, $|R(0)[cc]_{\bar{\mathbf{3}}}| \sim |R(0)[c\bar{c}]_{\mathbf{1}}|$. It is clear that the $|[qc]c\rangle$ states cannot be produced through the fragmentation mechanism on the LHCb.

4.4 Suppression of the radiative decay

An important issue is the rate for the heavier $|u(cc)\rangle$ state to decay radiatively to the spin-1/2 ground state $|[uc]c\rangle_{1/2^+}$. However, LHCb explicitly observed that the state they discovered decays weakly which means that the radiative decay of the LHCb state at 3621 MeV has to be strongly suppressed: The radiative lifetime has to be longer than approximately 50 fs in order that at least some of the LHCb 3621 MeV states would have survived and observed to decay weakly. A lifetime of 50 fs means that the transition rate $\Gamma(3621 \to 3520 + \gamma)$ has to be less than 0.01 eV. The energy of the photon emitted by the radiative transition is $\omega = 101$ MeV. The dependence of the transition rate on ω comes from (a) the phase space of the final state and (b) the dynamical suppression from the square of the matrix element of the electromagnetic current connecting the initial and final eigenstates.

For comparison, one can consider the measured radiative decay rate for $J/\psi \to \eta_c\gamma$ with photon energy $\omega = 115$ MeV [61]. The measured radiative decay rate for $J/\psi \to \eta_c\gamma$ is $\Gamma^{\rm exp} = 1.13 \pm 0.35$ keV. Note that the spatial wavefunctions of the J/ψ and the η_c are almost identical. In contrast, the initial and final state wavefunctions are very different. In the case of transition between the double-charm baryons $|q(cc)\rangle_{3/2^+} \to |[qc]c\rangle_{1/2^+} + \gamma$ the amplitude for radiative decay thus involves the matrix element $\langle f|\vec{J}_{\rm em}|i\rangle$ of the electromagnetic current between highly orthogonal hadronic eigenstates. In particular, the emission of the $\omega = 101$ MeV photon also has to interchange one of the charm quarks in the spin-1 (cc) diquark with the light quark q to form the spin-0 $[qc]$ diquark.

The matrix element in the LF framework involves the overlap of the current with nearly orthogonal three-body light-front wavefunctions $\psi_i(x, \vec{k}_\perp)$ and $\psi_f(x, \vec{k}_\perp)$ at the small 101 MeV momentum transfer. The matrix element thus must vanish as $(\omega r_{cc})^3$, where r_{cc}

characterizes the size of the radial wavefunctions. This gives a strong suppression of the rate of $(\omega r_{cc})^6$ relative to that of radiative charmonium decays.

According to Ref. [62], $r_{J/\psi} \sim 0.39\,\mathrm{fm} \simeq 2\,\mathrm{GeV}^{-1}$. As a first estimate, we will assume that the characteristic radial size of the charm diquark cc in the double-charm baryons is the same as that of the J/ψ, $r_{cc} \sim r_{J/\psi}$, resulting in $(\omega r_{cc})^6 \sim 6 \times 10^{-5}$. In comparison with the 1 keV $J/\psi \to \eta_c \gamma$ decay width, this would give a radiative transition rate for $|q(cc)\rangle_{3/2^+} \to |[qc]c\rangle_{1/2^+} + \gamma$ of order 0.06 eV and thus a radiative transition lifetime of 10 fs. A radiative lifetime of this order would not prevent the LHCb from observing the weak decay of the $|q(cc)\rangle$ double-charm baryon at 3621 MeV. In this case LHCb might be able to observe some radiative events $|[qc]c\rangle_{1/2^+} + \gamma$, where the $|[qc]c\rangle_{1/2^+}$ at 3520 MeV decays weakly.

It is also possible that the 3621 MeV state observed by LHCb is a $J^P = 1/2^+$ double-charm baryon state $|q(cc)\rangle_{1/2^+}$, rather than $J^P = 3/2^+$ since we have assumed that it is a bound state of a spin-1/2 quark and a spin-1 (cc) diquark. In this case the spin-1 photon needs to be emitted with orbital angular momentum $L = 1$ to conserve parity in the radiative decay of the 3621 MeV state $|q(cc)\rangle_{1/2^+}$ to the 3520 MeV state $|[qc]c\rangle_{1/2^+}$. This would give an additional factor of v^2 in the phase space for the radiative transition rate where $v \simeq \omega/M \sim 1/35$ is the recoil velocity of the 3520 MeV double-charm baryon. This additional suppression of the rate implies that the lifetime of the radiative transition would then be increased to be of order 12000 fs.

We have also done a comparison with the radiative transition rates between the $J^P = 1^-$ charmonium S states analyzed in the classic paper by Feinberg and Sucher [63], such as the estimated 10 keV transition rate between the $\psi(2S)(3686\,\mathrm{MeV})$ and the $J/\psi(3097\,\mathrm{MeV})$. The transition energy in our case is 101 MeV, compared to the transition energy between the $\psi(2S)(3686\,\mathrm{MeV})$ and the $J/\psi(3097\,\mathrm{MeV})$ of 589 MeV – a relative reduction in the photon transition energy of $101/589 \sim 1/6$. This factor enters at the third power in the matrix element of the spin current in Eq. (9) of Ref. [63] through the overlap of radial wavefunctions, i.e. the spherical Bessel function $j_0(kr/2)$. In addition, one has to take into account the additional suppression of electromagnetic transitions between the $q(cc)$ and

$[qc]c$ configurations when extrapolating to double-charm baryons.

The above discussion is clearly only a first estimate. A rigorous treatment of the transition radiative decay rate between double-charm baryons with diquarks of different spin and composition is clearly necessary.

We also note that LHCb may be able to detect radiative transitions involving double-charm baryons which have higher masses and higher spin. The observation of the 3520 MeV state $|[uc]c\rangle_{1/2^+}$ with a significant transverse momentum kick from photon emission from a heavy double charm state would be an important confirmation of our picture. Because of this, we suggest that LHCb conduct such a search.

Still, there might be intrinsic charm in the wave function at LHC. The contribution from the double intrinsic charm should be suppressed due to the kinematics of the LHCb experiment: Making the naive assumption that the momentum is split evenly between all final states and taking into account that the hadron identification efficiency for pions and kaons is degraded above $100\,\mathrm{GeV}/c$ [64, 65], the analysis looses sensitivity around $p(\Xi_{cc}^{++}) \approx 600\,\mathrm{GeV}/c$, i.e. $x_F \approx 0.15$ and $x_F \approx 0.09$ for the 8 GeV and 13 GeV analysis, respectively. This range of values for x_F corresponds to the rapidity region $2 < y < 5$ in which the LHCb detector operates [66]. Note that in contrast to SELEX, LHCb is a collider experiment where the acceptance excludes the detection of events close to the beam axis.

4.5 Lifetime difference

There is still an unexplained difference in lifetimes. Indeed, if we compare $\tau(\Xi_{cc}^{++}) = 256^{+24}_{-22}(\mathrm{stat}) \pm 14(\mathrm{sys})\,\mathrm{fs}$ as measured by LHCb with the upper limit of the $\tau(\Xi_{cc}^{+}) < 33\,\mathrm{fs}$ at 90% confidence level, we can easily find that the lifetime difference is higher than previously predicted, $\tau(\Xi_{cc}^{++})/\tau(\Xi_{cc}^{+}) \approx 2.5 - 4$ (cf. Refs. [54, 67]). However, none of the predictions, neither $\tau(\Xi_{cc}^{++}) = 460 \pm 50\,\mathrm{fs}$ [54] nor $\tau(\Xi_{cc}^{++}) = 185\,\mathrm{fs}$ [67] fits to the experimentally measured value of $\tau(\Xi_{cc}^{++})$. In Ref. [68] a value $\tau(\Xi_{cc}^{++}) = 298\,\mathrm{fs}$ was recently obtained which is very close to the experimental value (cf. Table 3). Also, the ratio $\tau(\Xi_{cc}^{++})/\tau(\Xi_{cc}^{+}) \sim 6.7$

Table 3: Theoretically predicted and the experimentally measured Ξ_{cc} baryon lifetime values

lifetime (fs)	Kiselev [54]	Karliner [67]	Cheng [68]	Exp.
$\tau(\Xi_{cc}^{+})$	160 ± 50	53	44	SELEX [8] < 33 (90% C.L.)
$\tau(\Xi_{cc}^{++})$	460 ± 50	185	298	LHCb [51] 256^{+38}_{-36}

was calculated. Using this ratio and the experimental value of $\tau(\Xi_{cc}^{++})$ we find $\tau(\Xi_{cc}^{+}) \sim 38\,\text{fs}$. This value is again close to the SELEX value.

Using the total integrated luminosity of $9\,\text{fb}^{-1}$ at center-of-mass energies of 7, 8, and 13 TeV and the decay mode $\Xi_{cc}^{+} \to \Lambda_c^{+} K^{-} \pi^{+}$, no significant signal is observed in the mass range from 3.4 to $3.8\,\text{GeV}/c^2$ and assumed lifetime between 40 and 160 fs, as reported in the recent LHCb publication [69].

It is also interesting to note that the LHCb result $\tau(\Omega_c^0) = 268 \pm 24 \pm 10 \pm 2\,\text{fs}$ [70] for the lifetime is in disagreement with the respective lifetime measured by fixed-target experiments (cf. Table 4).

Table 4: Ω_c^0 baryon lifetime values measured by fixed-target experiments

Experiment	lifetime (fs)	Number of events
FOCUS [72]	$72 \pm 11 \pm 11$	64
WA89 [73]	$55^{+13\,+18}_{-11\,-23}$	86
E687 [74]	$86^{+27}_{-20} \pm 28$	25
SELEX [75]	$65 \pm 13 \pm 9$	83

4.6 Production of the double heavy baryons at the AFTER@LHC

In Section 3.1 the application of the quark-duality principle for obtaining the production cross section was described. This logic can be fully applied to the calculation of the production cross section of the double charm baryons with a single minor difference. In contrast to the $Q\bar{Q}$ pair, the QQ pair has $3 \times 3 = (\bar{3} + 6)$ color components, consisting of a color antitriplet state and a color sextet. The probability that a QQ pair forms an antitriplet state is $\bar{3}/(\bar{3} + 6) = 1/3$. Therefore, in case of the doubly charmed baryon the cross section will be

$$\sigma(cc) = \frac{1}{3} f_{cc} \sigma_{icc}, \tag{30}$$

where f_{cc} is the fragmentation ratio of the cc pair described by Eq. (13). Obviously, the same logic can be applied to bc and bb pairs. It is interesting to compare our predictions with the single intrinsic charm mechanism predictions given in Ref. [71] (cf. Table 5).

Table 5: Baryonic cross sections

Baryon type	Single IC [71](pb)	Double IC (pb)
Ξ_{cc}	4.3×10^4	9.4×10^4
Ξ_{bc}	8.95	2.6×10^2
Ξ_{bb}	3.1×10^{-2}	50

5 The charm production in fixed-target experiments with the intrinsic charm from the target

> "I have every respect for your deductions, but you are wrong, completely and absolutely, and without any doubt."
>
> Tove Jansson,
> *Finn Family Moomintroll*

The possibility of the production of charm hadrons via the intrinsic charm mechanism from the target was proposed in Refs. [76, 77].

Recently, the LHCb collaboration presented the first measurement of charm production in the fixed-target configuration at the LHC [78]. The production of J/ψ and D^0 mesons is studied with beams of protons of different energies colliding with gaseous targets of helium and argon with nucleon–nucleon centre-of-mass energies of $\sqrt{s} = 86.6$ and 110.4 GeV, respectively. The J/ψ and D^0 production cross-sections in pHe collisions in the rapidity range $[2, 4.6]$ are found to be $\sigma(J/\psi) = 652 \pm 33 \pm 42\,\text{nb}$ per nucleon and $\sigma(D^0) = 80.8 \pm 2.4 \pm 6.3\,\mu\text{b}$ per nucleon, where the first uncertainty is statistical and the second is systematic. Providing an analysis of the production of D^0 mesons with the intrinsic charm from the target, LHCb reported no evidence for a substantial intrinsic charm content of the nucleon [78]. This result brings special attention to the topic.

In this chapter we discuss the beautiful prediction of the intrinsic charm model for the charm production in the fixed-target experiments with the intrinsic charm coming from the target. In addition, we show that based on a misunderstanding of the kinematics of the intrinsic charm from the target in the laboratory frame the LHCb/SMOG result is in contradiction to the properties of the intrinsic charm model.

5.1 The kinematic distributions and cross sections of the charm

The kinematic limits on the energy and the longitudinal momentum of the charm state formed by the intrinsic charm from the target are given by (cf. Appendix B)

$$E_{lab} = \frac{1}{2m_{tar}}(m_{pro}^2 + m_{tar}^2), \quad p_{lab} = \frac{1}{2m_{tar}}(m_{pro}^2 - m_{tar}^2). \tag{31}$$

These expressions depend solely on the two masses m_{pro} and m_{tar} of projectile and target and no longer on the beam energy.

Upon combining Eqs. (3) and (B.8) we can find the momentum distribution and the distribution of the rapidity difference $\Delta y = y - y_{tar}$ (in case of the target $y_{tar} = 0$) in the laboratory frame (cf. Fig. 10).

Using Eqs. (4) and (13) and the inelastic cross sections $\sigma_{pp}^{inel}(p_{\text{beam}} = 200\,\text{GeV}) \approx 32\,\text{mb}$ [79] and $\sigma_{pp}^{inel}(\sqrt{s} = 115\,\text{GeV}) \approx 37\,\text{mb}$ we can finally estimate respective production cross sections at the fixed-target program at STAR[4]

$$\sigma(\Xi_{cc}) \approx 75\,\text{nb}$$
$$\sigma(J/\psi) \approx 28\,\text{nb}$$

and at the AFTER@LHC

$$\sigma(\Xi_{cc}) \approx 65\,\text{nb}$$
$$\sigma(J/\psi) \approx 29\,\text{nb}.$$

5.2 Discussion of the LHCb/SMOG result

Using Eq. (B.8) we can obtain the kinematic limit (i.e. $x_F = 1$) of the open charm produced by the intrinsic charm mechanism from the target in the laboratory frame, $y < 0.6$ and $p_L \sim 1.2 - 1.3\,\text{GeV}/c$. By a straightforward calculation it was shown that in case of the production of intrinsic charm from the target, charm hadrons have a maximum momentum

[4]For the double charm baryons we provide the upper limits. For J/ψ we provide estimates based on experimental data [10].

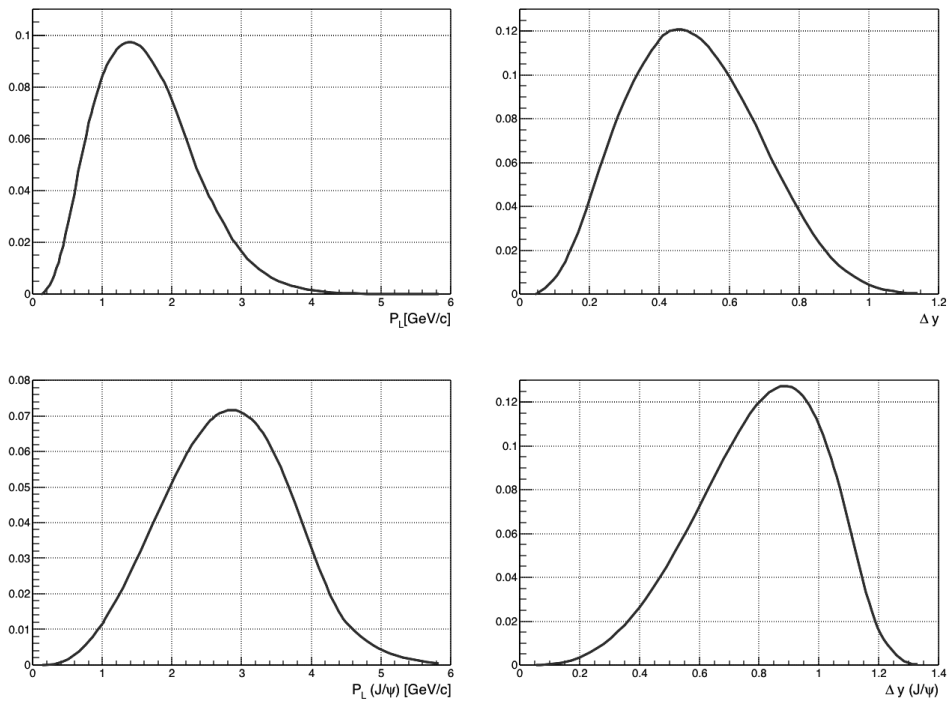

Figure 10: The upper panels show the prediction for the Ξ_{cc} momentum distribution (left panel) and for the distribution of the rapidity difference (right panel) in the laboratory frame. The bottom panels show the prediction for the J/ψ momentum distribution (left panel) and for the distribution of the rapidity difference (right panel) in the laboratory frame.

in the laboratory frame of only a few GeV/c and a rapidity $y < 2$. This result is in perfect agreement with predictions from the intrinsic charm model about the Δy region for the charm state, $\Delta y = y - y_{\rm tar}(y_{\rm tar} = 0) < 2$. In other words, the LHCb collaboration provided an analysis outside the signal region.

Moreover, the LHCb collaboration made a mistake even in the calculation in the center-of-mass system. Using an approximation for the fraction x of the nucleon momentum carried by the target parton,

$$x \simeq \frac{2m_c}{\sqrt{s_{NN}}} \exp(-y^*), \tag{32}$$

where $m_c = 1.28\,\mathrm{GeV}/c^2$ is the mass of the c quark and y^* is the center-of-mass rapidity, they found that the LHCb acceptance gives access to the large Bjorken-x region of the nucleon target up to $x \sim 0.37$ for D^0 mesons. However, it is easy to see that this equation is not fully correct. Using the standard Feynman-x notation in the center-of-mass system $x \approx \frac{2m_T}{\sqrt{s}} \sinh(y^*)$ (cf. Eq. (47.43) in Ref. [80]) and taking into account that $\sinh(y^*) \approx -\exp(-y^*)/2$ for large negative values of y^*, one finally obtains $x \approx -\frac{m_T}{\sqrt{s}} \exp(-y^*)$.

6 Results

"Well, that really is the last word in madness."

Tove Jansson,

Moominpappa at Sea

In this chapter we shall try to explain the significance of the results introduced in this thesis.

The associate production of the quarkonium were investigated in the many theoretical and experimental researches. However, we have shown that the NA3 data is puzzling and does not allow for a simple interpretation. We found that the calculation of the double J/ψ production cross section is not very useful for the identification of the production mechanism. Instead, we have pointed out that the kinematic distributions provide opportunities for the COMPASS experiment using the π^- beam of the SPS (CERN) at $190\,\mathrm{GeV}/c$ to measure the effect of the intrinsic charm mechanism or to identify the production mechanism.

We investigated the double intrinsic heavy quark mechanism for the double-quarkonium production in the high Feynman-x region at the AFTER@LHC experiment. In this particular case the production of the double quarkonium plays a special role as it provides direct access to the double heavy quark probabilities P_{icc}, P_{icb} and P_{ibb}. The x_F distribution for double-quarkonium production in proton beam events has not yet been measured (cf. also a comment at the end of the third paragraph in the Introduction of Ref. [12]). Therefore, our estimates cannot be compared to existing data but wait for future confirmation by experiments like AFTER@LHC, for which we give numerical values.

Since the publication of first evidences for the existence of doubly charmed baryons by the SELEX collaboration, this result became probably the most intriguing and controversial one in modern baryonic physics. The reason for this is that perturbative QCD can explain neither the SELEX production rate nor the x_F distribution. Using both theoretical

and experimental arguments, we have shown that the SELEX and the LHCb results for the production of doubly charmed baryons can both be correct. We have compared the data for double J/ψ production observed by the NA3 experiment and the SELEX result for Ξ_{cc}^+ production at high Feynman-x_F. We have found that the NA3 data strongly complement the SELEX production rate for the spin-1/2 $|[dc]c\rangle$ state. In contrast, LHCb has most likely discovered the heavier $|u(cc)\rangle$ produced by gluon–gluon fusion $gg \to c\bar{c}c\bar{c}$ at $x_F \sim 0$. The application of supersymmetric algebra to hadron spectroscopy, together with the intrinsic charm mechanism for the hadroproduction of heavy hadrons at large x_F, can thus resolve the apparent conflict between measurements of double-charm baryons by the SELEX fixed-target experiment and the LHCb experiment at the LHC collider. The mass difference of the two double-charm baryons reflects the distinct spins of the underlying diquarks.

An important conclusion from our study is that the natural kinematic domain for producing novel hadronic bound states, such as multi-heavy quark hadrons and the tetraquarks predicted by superconformal algebra, is the domain of large Feynman-x. In this domain, the constituents of the higher Fock states of the projectile, which are comoving at the same rapidity, can coalesce to produce a wide variety of color-singlet hadrons.

We have shown why the state $|[qc]c\rangle_{1/2^+}$ is favorably produced at high x_F within the kinematics of the SELEX acceptance, and conversely, why its production is unfavorable in the LHC acceptance.

We investigated the beautiful prediction of the intrinsic charm mechanism. The charm particles are produced from the target with an approximate mean value for the momentum of about a few GeV/c. Such "soft" final states can be observed at the current and future fixed-target experiments. The production cross sections are presented.

We have also shown that the LHCb/SMOG result is based on a misunderstanding of the kinematics of the intrinsic charm. Moreover, the investigation of the production of charmed hadrons with intrinsic charm from the target at the LHCb/SMOG fixed-target program is fundamentally unfeasible.

7 Appendix A

The SELEX Λ_c^+ sample

The SELEX double charm baryon analysis began with a sample of Λ_c^+ single-charm baryons decaying to $pK^-\pi^+$. This Λ_c^+ sample containing the same 1630 events events was used to measure the Λ_c^+ lifetime [48,49]. The sample is a part of 1979 ± 71 signal events for Λ_c^+ [53] collected by the SELEX experiment with the negative Σ^- and π^- beams at $600\,\mathrm{GeV}/c$ and positive proton beam at $540\,\mathrm{GeV}/c$. The corrected number of events for Σ^-, proton and π^- beams are presented in Figures A.1, A.2 and A.3.

SELEX reported that the double charm candidates were observed only in Σ^- and proton samples. To obtain the production ratio we use only these samples. It is easy to see that the ratio will be even smaller if we include also the π^- sample.

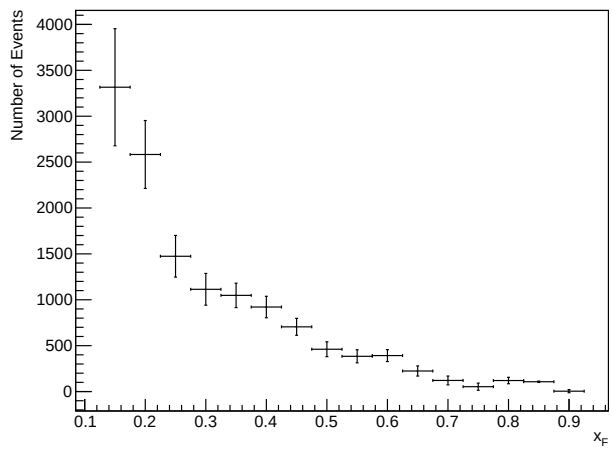

Figure A.1: Λ_c^+ x_F distribution of the corrected number of events for the Σ^- beam.

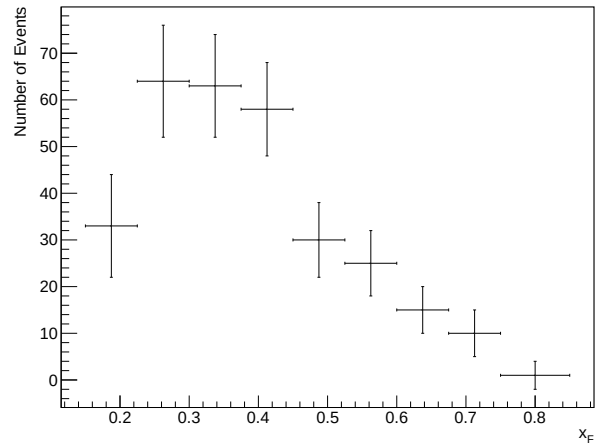

Figure A.2: Λ_c^+ x_F distribution of the corrected number of events for the proton beam.

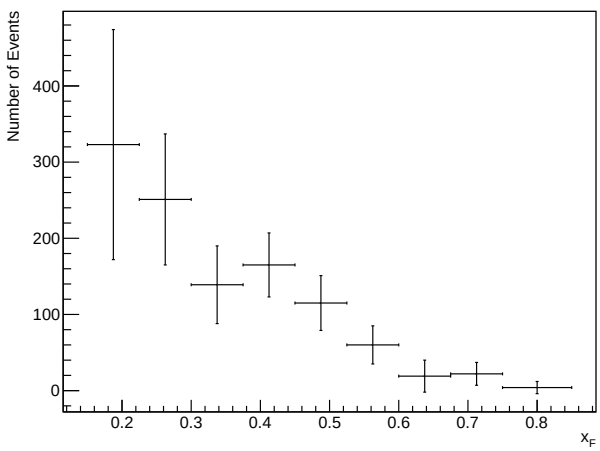

Figure A.3: Λ_c^+ x_F distribution of the corrected number of events for the π^- beam.

8 Appendix B

Derivation of the kinematic limit

Calculation of the Center of Mass System energy

Given an invariant energy $\sqrt{s}$, one can easily calculate the energies in the laboratory frame, the center-of-mass frame and of course in a lot of different other frames. Starting from

$$s = (p_P + p_T)^2 = p_P^2 + 2p_P p_T + p_T^2 = m_P^2 + 2p_P p_T + m_T^2 \tag{B.1}$$

we first can calculate in the laboratory system where $p_T = (m_T; 0, 0, 0)$. One obtains

$$s = m_P^2 + m_T^2 + 2E_P^{\rm lab} m_T \tag{B.2}$$

For the center-of-mass system, however, we have $\vec{p}_P + \vec{p}_T = \vec{0}$ ($\Rightarrow \vec{p}_P = -\vec{p}_T =: \vec{p}$) and, therefore, $\sqrt{s} = E_P + E_T$ where $E_P = (m_P^2 + \vec{p}^{\,2})^{1/2}$, $E_T = (m_T^2 + \vec{p}^{\,2})^{1/2}$. Inserting these energies we obtain

$$\sqrt{m_P^2 + \vec{p}^{\,2}} + \sqrt{m_T^2 + \vec{p}^{\,2}} = \sqrt{s}, \tag{B.3}$$

and this equation can be solved by two-fold squaring,

$$\begin{aligned}
2\sqrt{m_P^2 + \vec{p}^{\,2}}\sqrt{m_T^2 + \vec{p}^{\,2}} &= s - m_P^2 - m_T^2 - 2\vec{p}^{\,2} \\
4(m_P^2 + \vec{p}^{\,2})(m_T^2 + \vec{p}^{\,2}) &= (s - m_P^2 - m_T^2 - 2\vec{p}^{\,2})^2 \\
4\vec{p}^{\,4} + 4\vec{p}^{\,2}(m_P^2 + m_T^2) + 4m_P^2 m_T^2 &= (s - m_P^2 - m_T^2)^2 - 4\vec{p}^{\,2}(s - m_P^2 - m_T^2) + 4\vec{p}^{\,4} \\
4s\vec{p}^{\,2} &= (s - m_P^2 - m_T^2)^2 - 4m_P^2 m_T^2 \;=\; \lambda(s, m_P^2, m_T^2),
\end{aligned} \tag{B.4}$$

where $\lambda(x, y, z) = x^2 + y^2 + z^2 - 2xy - 2xz - 2yz$ is Källén's function. Given s by Eq. (B.2), one can proceed to calculate the square of the three-momentum to be

$$\begin{aligned}
\vec{p}^{\,2} &= \frac{\lambda(m_P^2 + m_T^2 + 2E_P m_T, m_P^2, m_T^2)}{4(m_P^2 + m_T^2 + 2E_P^{\rm lab} m_T)} = \frac{4((E_P^{\rm lab})^2 - m_P^2)m_T^2}{4(m_P^2 + m_T^2 + 2E_P^{\rm lab} m_T)} = \\
&= \frac{((E_P^{\rm lab})^2 - m_P^2)m_T^2}{m_P^2 + m_T^2 + 2E_P^{\rm lab} m_T} \approx \frac{(E_P^{\rm lab})^2 m_T^2}{2E_P^{\rm lab} m_T} = \frac{1}{2} E_P^{\rm lab} m_T.
\end{aligned} \tag{B.5}$$

Lorentz transformations

In order to get from one system to another, four-vectors have to be multiplied by Lorentz matrices. The Lorentz matrix which puts the general target four-vector $p_T = (E_T; -\vec{p})$ in the CMS to rest is given by

$$(\Lambda^{\mu}{}_{\nu}(E_T; -\vec{p})) = \Lambda(p_T) = \begin{pmatrix} E_T/m_T & \vec{p}^{\,T}/m_T \\ \vec{p}/m_T & \mathbb{1} + \vec{p}\vec{p}^{\,T}/m_T/(E_T + m_T) \end{pmatrix} \tag{B.6}$$

where $m_T^2 = E_T^2 - \vec{p}^{\,2}$. The upper index T stands for transposition of the (column) three-vector $\vec{p}$. It can easily be seen that $\Lambda(p_T)p_T = (m_T; \vec{0})^T$. Assuming that J/ψ takes over a ratio $x \in [0, 1]$ of the three-momentum $\vec{p}$ (for $x > 0$ from the projectile, for $x < 0$ from the target) and applying the Lorentz transformation to the corresponding four-vector $p_\psi = (E_\psi; x\vec{p})$ with $E_\psi^2 = m_\psi^2 + x^2\vec{p}^{\,2}$, one obtains a value for the four-vector in the laboratory frame, i.e. the frame where p_T is at rest. The result reads

$$\begin{aligned} E_\psi^{\text{lab}} &= \frac{1}{m_T}\left(\sqrt{\vec{p}_T^{\,2} + m_T^2}\sqrt{x^2\vec{p}_T^{\,2} + m_\psi^2} - x\vec{p}_T^{\,2}\right), \\ \vec{p}_\psi^{\,\text{lab}} &= \frac{\vec{p}_T}{m_T}\sqrt{x^2\vec{p}_T^{\,2} + m_\psi^2} - x\vec{p}_T\left(1 + \frac{\vec{p}_T^{\,2}}{m_T(m_T + \sqrt{\vec{p}_T^{\,2} + m_T^2})}\right). \end{aligned} \tag{B.7}$$

Taking into account that the three-momenta are usually much larger than the masses, we can expand into $m_T^2/\vec{p}^{\,2}$ and $m_\psi^2/\vec{p}^{\,2}$ to $x < 0$ (target) and obtain the maximum values of energy and momentum of the charm in the laboratory frame

$$E_\psi^{\text{lab}} = \frac{1}{2m_T}\left(m_\psi^2 + m_T^2\right), \qquad \vec{p}_\psi^{\,\text{lab}} = \frac{\vec{p}}{2m_T|\vec{p}\,|}\left(m_\psi^2 - m_T^2\right). \tag{B.8}$$

This last expression depends solely on the two masses m_ψ and m_T and no longer on the beam energy.

9 Appendix C

We already investigated possible contribution from SPS and IC mechanisms, and we even mentioned the contribution from DPS. However, it is possible to produce a pair of J/ψ

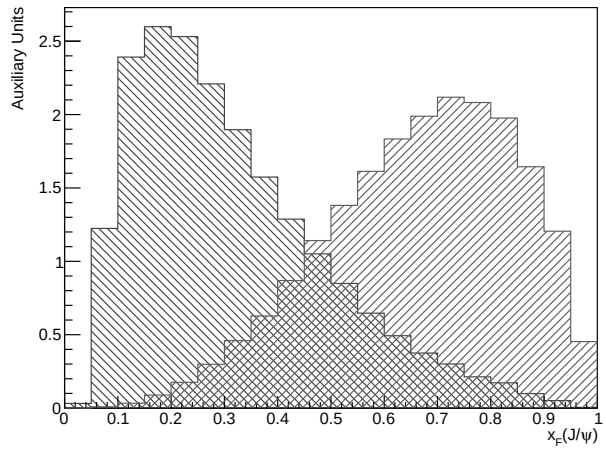

Figure C.1: Prediction for the x_F distributions of a single J/ψ for SPS (blue histogram to the left) and IC (red histogram to the right).

mesons also by SPS–IC interference. In this case one of the J/ψ comes from IC and the other from a standard pQCD SPS process like gluon–gluon fusion or quark–antiquark annihilation.

As the J/ψ from IC is produced at the "surface" of the hadron or nucleus, we assume that IC mechanism always contributes first. Starting from the x_F distributions in Fig. C.1 for single J/ψ from IC (red histogram to the right) or SPS (blue histogram to the left), the double J/ψ distribution for SPS–IC interference is calculated under this assumption to be as shown in Fig C.2. It is easy to see that the present region of double J/ψ in the NA3 data does not support this production mechanism very much.

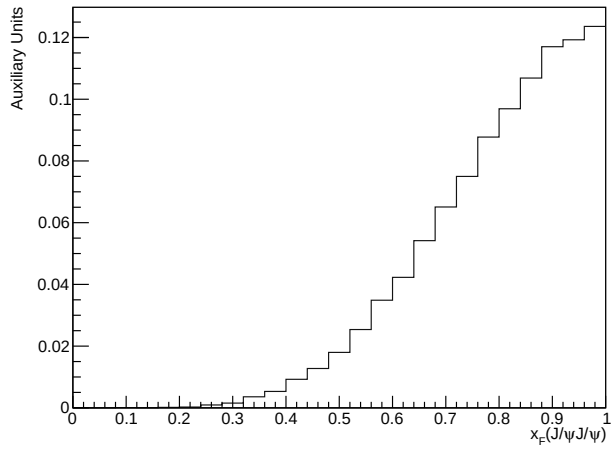

Figure C.2: Prediction for the x_F distributions of a J/ψ pair for SPS–IC interference.

References

[1] S.J. Brodsky, P. Hoyer, C. Peterson and N. Sakai, Phys. Lett. B **93** (1980) 451

[2] S. J. Brodsky, C. Peterson and N. Sakai, Phys. Rev. D **23** (1981) 2745

[3] S.J. Brodsky, J.C. Collins, S.D. Ellis, J.F. Gunion and A.H. Mueller, Snowmass Summer Study 1984:0227

[4] M. Franz, M.V. Polyakov and K. Goeke, Phys. Rev. **D62** (2000) 074024

[5] W.S. Lockman, T. Meyer, J. Rander, P. Schlein, R. Webb, S. Erhan and J. Zsembery, Phys. Lett. **B85** (1979) 443

[6] P. Chauvat *et al.* [R608 Collaboration], Phys. Lett. **B199** (1987) 304

[7] G. Bari *et al.*, Nuovo Cim. **A104** (1991) 1787

[8] M. Mattson *et al.* [SELEX Collaboration], Phys. Rev. Lett. **89** (2002) 112001

[9] A. Ocherashvili *et al.* [SELEX Collaboration], Phys. Lett. **B628** (2005) 18

[10] J. Badier *et al.* [NA3 Collaboration], Z. Phys. **C20** (1983) 101

[11] J. Badier *et al.* [NA3 Collaboration], Phys. Lett. **B114** (1982) 457

[12] R. Vogt and S.J. Brodsky, Phys. Lett. **B349** (1995) 569

[13] G. Aad *et al.* [ATLAS Collaboration], JHEP **1404** (2014) 172

[14] G. Aad *et al.* [ATLAS Collaboration], Eur. Phys. J. **C75** (2015) 229

[15] R. Aaij *et al.* [LHCb Collaboration], JHEP **1206** (2012) 141;
Addendum: [JHEP **1403** (2014) 108]

[16] R. Aaij *et al.* [LHCb Collaboration], Phys. Lett. **B707** (2012) 52

[17] V.M. Abazov *et al.* [D0 Collaboration], Phys. Rev. **D90** (2014) 111101

[18] V. Khachatryan *et al.* [CMS Collaboration], JHEP **1409** (2014) 094

[19] R. Aaij *et al.* [LHCb Collaboration], JHEP **1706** (2017) 047 [JHEP **1710** (2017) 068E]

[20] M. Aaboud *et al.* [ATLAS Collaboration], Eur. Phys. J. **C77** (2017) 76

[21] S. J. Brodsky, F. Fleuret, C. Hadjidakis and J. P. Lansberg,
Phys. Rept. **522** (2013) 239

[22] J. P. Lansberg, S. J. Brodsky, F. Fleuret and C. Hadjidakis,
Few Body Syst. **53** (2012) 11

[23] J. P. Lansberg *et al.*, EPJ Web Conf. **66** (2014) 11023

[24] A. Rakotozafindrabe *et al.*, PoS DIS **2013** (2013) 250

[25] S. J. Brodsky, A. Kusina, F. Lyonnet, I. Schienbein, H. Spiesberger and R. Vogt,
Adv. High Energy Phys. **2015** (2015) 231547

[26] J. F. Amundson, O. J. P. Eboli, E. M. Gregores and F. Halzen,
Phys. Lett. B **372** (1996) 127

[27] B. Humpert and P. Mery, Z. Phys. C **20** (1983) 83

[28] E. J. Eichten and C. Quigg, Phys. Rev. D **52** (1995) 1726

[29] J. Badier *et al.* [Saclay-CERN-College de France-Ecole Poly-Orsay Collaboration],
Nucl. Instrum. Meth. **175** (1980) 319

[30] T. Sjöstrand, S. Mrenna and P.Z. Skands, Comput. Phys. Commun. **178** (2008) 852

[31] H.S. Shao, Comput. Phys. Commun. **184** (2013) 2562

[32] H.S. Shao, Comput. Phys. Commun. **198** (2016) 238

[33] R.E. Ecclestone and D.M. Scott, Phys. Lett. **B120** (1983) 237

[34] R. Vogt, Nucl. Phys. **B446** (1995) 159

[35] P. Abbon *et al.* [COMPASS Collaboration], Nucl. Instrum. Meth. **A779** (2015) 69

[36] M. Aghasyan *et al.* [COMPASS Collaboration], Phys. Rev. Lett. **119** (2017) 112002

[37] C. Riedl, 23rd International Spin Symposium,
University of Ferrara, September 9–14, 2018

[38] B. Humpert and P. Mery, Phys. Lett. **B124** (1983) 265

[39] J. P. Lansberg and H. S. Shao, Nucl. Phys. B **900** (2015) 273

[40] D. d'Enterria and A.M. Snigirev, Nucl. Phys. **A932** (2014) 296

[41] M. Rinaldi, S. Scopetta, M. Traini and V. Vento, Eur. Phys. J. **C78** (2018) 781

[42] M. M. Block and F. Halzen, Phys. Rev. D **86** (2012) 014006

[43] R. Vogt and S. J. Brodsky, Nucl. Phys. B **438** (1995) 261

[44] M. E. Mattson, "Search for Baryons with Two Charm Quarks," doi:10.2172/1420963

[45] M.A. Moinester *et al.* [SELEX Collaboration], Czech. J. Phys. **53** (2003) B201

[46] J. Engelfried [SELEX Collaboration], Nucl. Phys. **A752**, 121 (2005)

[47] J. Engelfried [SELEX Collaboration], Proceedings of the International Conference on Heavy Quarks and Leptons (HQL 06), Munich, Germany, 16–20 October 2006, eConf C **0610161** (2006) 003

[48] A. Kushnirenko *et al.* [SELEX Collaboration], Phys. Rev. Lett. **86**, 5243 (2001)

[49] A. Y. Kushnirenko, "Precision Measurements of the Λ_c^+ and D^0 Lifetimes," doi:10.2172/1421447

[50] R. Aaij *et al.* [LHCb Collaboration], Phys. Rev. Lett. **119** (2017) 112001

[51] R. Aaij *et al.* [LHCb Collaboration], Phys. Rev. Lett. **121** (2018) no.5, 052002

[52] R. Aaij *et al.* [LHCb Collaboration], Phys. Rev. Lett. **121** (2018) no.16, 162002

[53] F.G. Garcia *et al.* [SELEX Collaboration], Phys. Lett. **B528** (2002) 49

[54] V.V. Kiselev and A.K. Likhoded,
Phys. Usp. **45** (2002) 455 [Usp. Fiz. Nauk **172** (2002) 497]

[55] M. Mangano, H. Satz and U. Wiedermann (Eds.),
CERN Yellow report, CERN-2004-009, 2004

[56] H.G. Dosch, G.F. de Téramond and S.J. Brodsky, Phys. Rev. **D91** (2015) 085016

[57] H.G. Dosch, G.F. de Téramond and S.J. Brodsky,
Phys. Rev. **D92** (2015) 074010; Phys. Rev. **D95** (2017) 034016

[58] S.J. Brodsky, G.F. de Téramond, H.G. Dosch and C. Lorcé,
Phys. Lett. **B759** (2016) 171

[59] J.G. Körner, M. Krämer and D. Pirjol, Prog. Part. Nucl. Phys. **33** (1994) 787

[60] R. Aaij *et al.* [LHCb Collaboration], JHEP **1312** (2013) 090

[61] D. Ebert, R.N. Faustov and V.O. Galkin, Phys. Rev. D **67** (2003) 014027

[62] K. Nochi, T. Kawanai and S. Sasaki, Phys. Rev. D **94** (2016) no. 11, 114514

[63] G. Feinberg and J. Sucher, Phys. Rev. Lett. **35** (1975) 1740

[64] M. Adinolfi *et al.* [LHCb RICH Group], Eur. Phys. J. C **73** (2013) 2431

[65] A. Papanestis *et al.* [LHCb RICH Collaboration],
Nucl. Instrum. Meth. A **876** (2017) 221

[66] A.A. Alves, Jr. *et al.* [LHCb Collaboration], JINST **3** (2008) S08005

[67] M. Karliner and J.L. Rosner, Phys. Rev. **D90** (2014) 094007

[68] H. Y. Cheng and Y. L. Shi, Phys. Rev. D **98** (2018) no.11, 113005

[69] R. Aaij *et al.* [LHCb Collaboration],
Sci. China Phys. Mech. Astron. **63** (2020) no.2, 221062

[70] R. Aaij *et al.* [LHCb Collaboration], Phys. Rev. Lett. **121** (2018) no.9, 092003

[71] G. Chen, X. G. Wu, J. W. Zhang, H. Y. Han and H. B. Fu,
Phys. Rev. D **89** (2014) no.7, 074020

[72] J. M. Link *et al.* [FOCUS Collaboration], Phys. Lett. B **561** (2003) 41

[73] M. I. Adamovich *et al.* [WA89 Collaboration], Phys. Lett. B **358** (1995) 151

[74] P. L. Frabetti *et al.* [E687 Collaboration], Phys. Lett. B **357** (1995) 678

[75] M. Iori *et al.* [SELEX Collaboration], hep-ex/0701021

[76] S. J. Brodsky, V. A. Bednyakov, G. I. Lykasov, J. Smiesko and S. Tokar, Prog. Part. Nucl. Phys. **93** (2017) 108

[77] S.J. Brodsky, Workshop on LHCb Heavy Ion and Fixed Target physics, CERN, January 9–10, 2017

[78] R. Aaij *et al.* [LHCb Collaboration], Phys. Rev. Lett. **122** (2019) 132002

[79] A. Schiz *et al.*, Phys. Rev. D **24** (1981) 26

[80] M. Tanabashi *et al.* [Particle Data Group], Phys. Rev. **D98** (2018) 030001

[81] A. Kulesza and W.J. Stirling, Phys. Lett. **B475** (2000) 168

[82] K.C. Meehan [STAR Collaboration], J. Phys. Conf. Ser. **742** (2016) 012022

[83] R. Aaij *et al.* [LHCb Collaboration], JINST **7** (2012) P01010

[84] R. Aaij *et al.* [LHCb Collaboration], Int. J. Mod. Phys. A **30** (2015) no.07, 1530022

Publications

CURRICULUM VITAE

Name:	Sergey Koshkarev
Date of birth:	September 3rd, 1983
Nationality:	Russian Federation
Phone:	+372 5822 4594
E-mail:	sergey.koshkarev@ut,ee, koshkarev.sergey@gmail.com

Education

2001–2007	M.Sc. in Particle Physics and Cosmology,
	Moscow Engineering and Physics Institute (MEPhI)
2007–2009	Fermilab Fellow at the Institute for High Energy Physics, Russia
2009–2011	Fermilab Fellow at the Universidad de Cantabria, Spain
2016–2020	Ph.D. in Particle Physics Phenomenology, University of Tartu, Estonia

Employment

2011–2012	Researcher at the Speech Technology Center, St. Petersburg, Russia
2012–2015	Leading EDI Specialist and Software Developer at
	Intelligent Audit, St. Petersburg, Russia
2016–	EDI Developer at Kuehne & Nagel, Tallinn, Estonia

List of publications

- A. Rakitin, S. Koshkarev, "Hadronic B_c decays as a test of B_c cross section," *Phys. Rev. D* **81** (2010) 014005
- S. Koshkarev, V. Anikeev, "Production of the doubly charmed baryons at the SELEX experiment – The double intrinsic charm approach," *Phys. Lett. B* **765** (2017) 171
- S. Koshkarev, "Production of the Doubly Heavy Baryons, B_c Meson and the All-charm Tetraquark at AFTER@LHC with Double Intrinsic Heavy Mechanism," *Acta Phys. Polon. B* **48** (2017) 163

- S. Koshkarev, S. Groote, "Double quarkonium production at high Feynman-x," *Nucl. Phys. B* **915** (2017) 384

- S. Groote, S. Koshkarev, "Production of doubly charmed baryons nearly at rest," *Eur. Phys. J. C* **77** (2017) 509

- S. J. Brodsky, S. Groote, S. Koshkarev, "Resolving the SELEX–LHCb double-charm baryon conflict: the impact of intrinsic heavy-quark hadroproduction and supersymmetric light-front holographic QCD," *Eur. Phys. J. C* **78** (2018) 483

Conference presentations

- S. Koshkarev, S. Groote, "Signals of the double intrinsic heavy quark at the current experiments," *J. Phys. Conf. Ser.* **938** (2017) 012054

- S. Koshkarev, S. Groote, "Resolving the SELEX–LHCb double-charm baryon conflict: the impact of intrinsic heavy-quark hadroproduction and supersymmetric light-front holographic QCD," *EPJ Web Conf.* **204** (2019) 08007

Preprints

- S. Koshkarev, "Phenomenological analysis of the possible impact of Double Parton Scattering in double J/ψ production at the COMPASS detector using the CERN π^- beam at 190 GeV/c," *arXiv:1909.06195 [hep-ph]*

- A. Gridin, S. Groote, A. Guskov, S. Koshkarev, "Feasibility study for the search of intrinsic charm at the COMPASS experiment and at the STAR fixed-target program," *arXiv:1901.01712 [hep-ph]*

- S. Groote, S. Koshkarev,
  "On the kinematic limit of the charm production in fixed-target experiments with the intrinsic charm from the target," *arXiv:1901.04193 [hep-ph]*

- S. Koshkarev, S. Groote,
  "Analysis of the baryonic state $|[qc]c\rangle$," *arXiv:1803.07034 [hep-ph]*

ELULOOKIRJELDUS

Nimi:	Sergey Koshkarev
Sünniaeg:	3. september 1983
Kodakondsus:	Venemaa
Telefon:	+372 5822 4594
E-mail:	sergey.koshkarev@ut,ee, koshkarev.sergey@gmail.com

Haridus

2001–2007	Osakestefüüsika ja kosmoloogia magister,
	Moscow Engineering and Physics Institute (MEPhI)
2007–2009	Fermilab teadur, Institute for High Energy Physics, Venemaa
2009–2011	Fermilab teadur, Universidad de Cantabria, Hispaania
2016–2020	Osakestefüüsika fenomenoloogia doktorant, Tartu Ülikool, Eesti

Teenus

2011–2012	Teadur, Speech Technology Center, St. Petersburg, Venemaa
2012–2015	Juhiv EDI asjatundja ja tarkvara arendaja,
	Intelligent Audit, St. Petersburg, Venemaa
2016–	EDI arendaja, Kuehne & Nagel, Tallinn, Eesti

Publikatsioonide loetelu

- A. Rakitin, S. Koshkarev, "Hadronic B_c decays as a test of B_c cross section," *Phys. Rev. D* **81** (2010) 014005
- S. Koshkarev, V. Anikeev, "Production of the doubly charmed baryons at the SELEX experiment – The double intrinsic charm approach," *Phys. Lett. B* **765** (2017) 171
- S. Koshkarev, "Production of the Doubly Heavy Baryons, B_c Meson and the All-charm Tetraquark at AFTER@LHC with Double Intrinsic Heavy Mechanism," *Acta Phys. Polon. B* **48** (2017) 163

- S. Koshkarev, S. Groote, "Double quarkonium production at high Feynman-x," *Nucl. Phys. B* **915** (2017) 384

- S. Groote, S. Koshkarev, "Production of doubly charmed baryons nearly at rest," *Eur. Phys. J. C* **77** (2017) 509

- S. J. Brodsky, S. Groote, S. Koshkarev, "Resolving the SELEX–LHCb double-charm baryon conflict: the impact of intrinsic heavy-quark hadroproduction and supersymmetric light-front holographic QCD," *Eur. Phys. J. C* **78** (2018) 483

Publitseeritud konverentsiettekanded

- S. Koshkarev, S. Groote, "Signals of the double intrinsic heavy quark at the current experiments," *J. Phys. Conf. Ser.* **938** (2017) 012054

- S. Koshkarev, S. Groote, "Resolving the SELEX–LHCb double-charm baryon conflict: the impact of intrinsic heavy-quark hadroproduction and supersymmetric light-front holographic QCD," *EPJ Web Conf.* **204** (2019) 08007

Eelpublikatsioonid

- S. Koshkarev, "Phenomenological analysis of the possible impact of Double Parton Scattering in double J/ψ production at the COMPASS detector using the CERN π^- beam at 190 GeV/c," *arXiv:1909.06195 [hep-ph]*

- A. Gridin, S. Groote, A. Guskov, S. Koshkarev, "Feasibility study for the search of intrinsic charm at the COMPASS experiment and at the STAR fixed-target program," *arXiv:1901.01712 [hep-ph]*

- S. Groote, S. Koshkarev,
  "On the kinematic limit of the charm production in fixed-target experiments with the intrinsic charm from the target," *arXiv:1901.04193 [hep-ph]*

- S. Koshkarev, S. Groote,
  "Analysis of the baryonic state $|[qc]c\rangle$," *arXiv:1803.07034 [hep-ph]*

DISSERTATIONES PHYSICAE UNIVERSITATIS TARTUENSIS

1. **Andrus Ausmees.** XUV-induced electron emission and electron-phonon interaction in alkali halides. Tartu, 1991.
2. **Heiki Sõnajalg.** Shaping and recalling of light pulses by optical elements based on spectral hole burning. Tartu, 1991.
3. **Sergei Savihhin.** Ultrafast dynamics of F-centers and bound excitons from picosecond spectroscopy data. Tartu, 1991.
4. **Ergo Nõmmiste.** Leelishalogeniidide röntgenelektronemissioon kiiritamisel footonitega energiaga 70–140 eV. Tartu, 1991.
5. **Margus Rätsep.** Spectral gratings and their relaxation in some low-temperature impurity-doped glasses and crystals. Tartu, 1991.
6. **Tõnu Pullerits.** Primary energy transfer in photosynthesis. Model calculations. Tartu, 1991.
7. **Olev Saks.** Attoampri diapasoonis voolude mõõtmise füüsikalised alused. Tartu, 1991.
8. **Andres Virro.** AlGaAsSb/GaSb heterostructure injection lasers. Tartu, 1991.
9. **Hans Korge.** Investigation of negative point discharge in pure nitrogen at atmospheric pressure. Tartu, 1992.
10. **Jüri Maksimov.** Nonlinear generation of laser VUV radiation for high-resolution spectroscopy. Tartu, 1992.
11. **Mark Aizengendler.** Photostimulated transformation of aggregate defects and spectral hole burning in a neutron-irradiated sapphire. Tartu, 1992.
12. **Hele Siimon.** Atomic layer molecular beam epitaxy of A^2B^6 compounds described on the basis of kinetic equations model. Tartu, 1992.
13. **Tõnu Reinot.** The kinetics of polariton luminescence, energy transfer and relaxation in anthracene. Tartu, 1992.
14. **Toomas Rõõm.** Paramagnetic H^{2-} and F^+ centers in CaO crystals: spectra, relaxation and recombination luminescence. Tallinn, 1993.
15. **Erko Jalviste.** Laser spectroscopy of some jet-cooled organic molecules. Tartu, 1993.
16. **Alvo Aabloo.** Studies of crystalline celluloses using potential energy calculations. Tartu, 1994.
17. **Peeter Paris.** Initiation of corona pulses. Tartu, 1994.
18. **Павел Рубин.** Локальные дефектные состояния в CuO_2 плоскостях высокотемпературных сверхпроводников. Тарту, 1994.
19. **Olavi Ollikainen.** Applications of persistent spectral hole burning in ultrafast optical neural networks, time-resolved spectroscopy and holographic interferometry. Tartu, 1996.
20. **Ülo Mets.** Methodological aspects of fluorescence correlation spectroscopy. Tartu, 1996.
21. **Mikhail Danilkin.** Interaction of intrinsic and impurity defects in CaS:Eu luminophors. Tartu, 1997.

22. **Ирина Кудрявцева.** Создание и стабилизация дефектов в кристаллах KBr, KCl, RbCl при облучении ВУФ-радиацией. Тарту, 1997.
23. **Andres Osvet.** Photochromic properties of radiation-induced defects in diamond. Tartu, 1998.
24. **Jüri Örd.** Classical and quantum aspects of geodesic multiplication. Tartu, 1998.
25. **Priit Sarv.** High resolution solid-state NMR studies of zeolites. Tartu, 1998.
26. **Сергей Долгов.** Электронные возбуждения и дефектообразование в некоторых оксидах металлов. Тарту, 1998.
27. **Kaupo Kukli.** Atomic layer deposition of artificially structured dielectric materials. Tartu, 1999.
28. **Ivo Heinmaa.** Nuclear resonance studies of local structure in $RBa_2Cu_3O_{6+x}$ compounds. Tartu, 1999.
29. **Aleksander Shelkan.** Hole states in CuO_2 planes of high temperature superconducting materials. Tartu, 1999.
30. **Dmitri Nevedrov.** Nonlinear effects in quantum lattices. Tartu, 1999.
31. **Rein Ruus.** Collapse of 3d (4f) orbitals in 2p (3d) excited configurations and its effect on the x-ray and electron spectra. Tartu, 1999.
32. **Valter Zazubovich.** Local relaxation in incommensurate and glassy solids studied by Spectral Hole Burning. Tartu, 1999.
33. **Indrek Reimand.** Picosecond dynamics of optical excitations in GaAs and other excitonic systems. Tartu, 2000.
34. **Vladimir Babin.** Spectroscopy of exciton states in some halide macro- and nanocrystals. Tartu, 2001.
35. **Toomas Plank.** Positive corona at combined DC and AC voltage. Tartu, 2001.
36. **Kristjan Leiger.** Pressure-induced effects in inhomogeneous spectra of doped solids. Tartu, 2002.
37. **Helle Kaasik.** Nonperturbative theory of multiphonon vibrational relaxation and nonradiative transitions. Tartu, 2002.
38. **Tõnu Laas.** Propagation of waves in curved spacetimes. Tartu, 2002.
39. **Rünno Lõhmus.** Application of novel hybrid methods in SPM studies of nanostructural materials. Tartu, 2002.
40. **Kaido Reivelt.** Optical implementation of propagation-invariant pulsed free-space wave fields. Tartu, 2003.
41. **Heiki Kasemägi.** The effect of nanoparticle additives on lithium-ion mobility in a polymer electrolyte. Tartu, 2003.
42. **Villu Repän.** Low current mode of negative corona. Tartu, 2004.
43. **Алексей Котлов.** Оксианионные диэлектрические кристаллы: зонная структура и электронные возбуждения. Tartu, 2004.
44. **Jaak Talts.** Continuous non-invasive blood pressure measurement: comparative and methodological studies of the differential servo-oscillometric method. Tartu, 2004.
45. **Margus Saal.** Studies of pre-big bang and braneworld cosmology. Tartu, 2004.

46. **Eduard Gerškevitš.** Dose to bone marrow and leukaemia risk in external beam radiotherapy of prostate cancer. Tartu, 2005.
47. **Sergey Shchemelyov.** Sum-frequency generation and multiphoton ionization in xenon under excitation by conical laser beams. Tartu, 2006.
48. **Valter Kiisk.** Optical investigation of metal-oxide thin films. Tartu, 2006.
49. **Jaan Aarik.** Atomic layer deposition of titanium, zirconium and hafnium dioxides: growth mechanisms and properties of thin films. Tartu, 2007.
50. **Astrid Rekker.** Colored-noise-controlled anomalous transport and phase transitions in complex systems. Tartu, 2007.
51. **Andres Punning.** Electromechanical characterization of ionic polymer-metal composite sensing actuators. Tartu, 2007.
52. **Indrek Jõgi.** Conduction mechanisms in thin atomic layer deposited films containing TiO_2. Tartu, 2007.
53. **Aleksei Krasnikov.** Luminescence and defects creation processes in lead tungstate crystals. Tartu, 2007.
54. **Küllike Rägo.** Superconducting properties of MgB_2 in a scenario with intra- and interband pairing channels. Tartu, 2008.
55. **Els Heinsalu.** Normal and anomalously slow diffusion under external fields. Tartu, 2008.
56. **Kuno Kooser.** Soft x-ray induced radiative and nonradiative core-hole decay processes in thin films and solids. Tartu, 2008.
57. **Vadim Boltrushko.** Theory of vibronic transitions with strong nonlinear vibronic interaction in solids. Tartu, 2008.
58. **Andi Hektor.** Neutrino Physics beyond the Standard Model. Tartu, 2008.
59. **Raavo Josepson.** Photoinduced field-assisted electron emission into gases. Tartu, 2008.
60. **Martti Pärs.** Study of spontaneous and photoinduced processes in molecular solids using high-resolution optical spectroscopy. Tartu, 2008.
61. **Kristjan Kannike.** Implications of neutrino masses. Tartu, 2008.
62. **Vigen Issahhanjan.** Hole and interstitial centres in radiation-resistant MgO single crystals. Tartu, 2008.
63. **Veera Krasnenko.** Computational modeling of fluorescent proteins. Tartu, 2008.
64. **Mait Müntel.** Detection of doubly charged higgs boson in the CMS detector. Tartu, 2008.
65. **Kalle Kepler.** Optimisation of patient doses and image quality in diagnostic radiology. Tartu, 2009.
66. **Jüri Raud.** Study of negative glow and positive column regions of capillary HF discharge. Tartu, 2009.
67. **Sven Lange.** Spectroscopic and phase-stabilisation properties of pure and rare-earth ions activated ZrO_2 and HfO_2. Tartu, 2010.
68. **Aarne Kasikov.** Optical characterization of inhomogeneous thin films. Tartu, 2010.
69. **Heli Valtna-Lukner.** Superluminally propagating localized optical pulses. Tartu, 2010.

70. **Artjom Vargunin.** Stochastic and deterministic features of ordering in the systems with a phase transition. Tartu, 2010.
71. **Hannes Liivat.** Probing new physics in e+e− annihilations into heavy particles via spin orientation effects. Tartu, 2010.
72. **Tanel Mullari.** On the second order relativistic deviation equation and its applications. Tartu, 2010.
73. **Aleksandr Lissovski.** Pulsed high-pressure discharge in argon: spectroscopic diagnostics, modeling and development. Tartu, 2010.
74. **Aile Tamm.** Atomic layer deposition of high-permittivity insulators from cyclopentadienyl-based precursors. Tartu, 2010.
75. **Janek Uin.** Electrical separation for generating standard aerosols in a wide particle size range. Tartu, 2011.
76. **Svetlana Ganina.** Hajusandmetega ülesanded kui üks võimalus füüsikaõppe efektiivsuse tõstmiseks. Tartu, 2011
77. **Joel Kuusk.** Measurement of top-of-canopy spectral reflectance of forests for developing vegetation radiative transfer models. Tartu, 2011.
78. **Raul Rammula**. Atomic layer deposition of HfO_2 – nucleation, growth and structure development of thin films. Tartu, 2011.
79. **Сергей Наконечный.** Исследование электронно-дырочных и интерстициал-вакансионных процессов в монокристаллах MgO и LiF методами термоактивационной спектроскопии. Тарту, 2011.
80. **Niina Voropajeva.** Elementary excitations near the boundary of a strongly correlated crystal. Tartu, 2011.
81. **Martin Timusk.** Development and characterization of hybrid electro-optical materials. Tartu, 2012, 106 p.
82. **Merle Lust.** Assessment of dose components to Estonian population. Tartu, 2012, 84 p.
83. **Karl Kruusamäe.** Deformation-dependent electrode impedance of ionic electromechanically active polymers. Tartu, 2012, 128 p.
84. **Liis Rebane.** Measurement of the $W \to \tau\nu$ cross section and a search for a doubly charged Higgs boson decaying to τ-leptons with the CMS detector. Tartu, 2012, 156 p.
85. **Jevgeni Šablonin.** Processes of structural defect creation in pure and doped MgO and NaCl single crystals under condition of low or super high density of electronic excitations. Tartu, 2013, 145 p.
86. **Riho Vendt**. Combined method for establishment and dissemination of the international temperature scale. Tartu, 2013, 108 p.
87. **Peeter Piksarv.** Spatiotemporal characterization of diffractive and non-diffractive light pulses. Tartu, 2013, 156 p.
88. **Anna Šugai.** Creation of structural defects under superhigh-dense irradiation of wide-gap metal oxides. Tartu, 2013, 108 p.
89. **Ivar Kuusik.** Soft X-ray spectroscopy of insulators. Tartu, 2013, 113 p.
90. **Viktor Vabson**. Measurement uncertainty in Estonian Standard Laboratory for Mass. Tartu, 2013, 134 p.

91. **Kaupo Voormansik.** X-band synthetic aperture radar applications for environmental monitoring. Tartu, 2014, 117 p.
92. **Deivid Pugal.** hp-FEM model of IPMC deformation. Tartu, 2014, 143 p.
93. **Siim Pikker.** Modification in the emission and spectral shape of photostable fluorophores by nanometallic structures. Tartu, 2014, 98 p.
94. **Mihkel Pajusalu**. Localized Photosynthetic Excitons. Tartu, 2014, 183 p.
95. **Taavi Vaikjärv.** Consideration of non-adiabaticity of the Pseudo-Jahn-Teller effect: contribution of phonons. Tartu, 2014, 129 p.
96. **Martin Vilbaste.** Uncertainty sources and analysis methods in realizing SI units of air humidity in Estonia. Tartu, 2014, 111 p.
97. **Mihkel Rähn.** Experimental nanophotonics: single-photon sources- and nanofiber-related studies. Tartu, 2015, 107 p.
98. **Raul Laasner.** Excited state dynamics under high excitation densities in tungstates. Tartu, 2015, 125 p.
99. **Andris Slavinskis.** EST Cube-1 attitude determination. Tartu, 2015, 104 p.
100. **Karlis Zalite**. Radar Remote Sensing for Monitoring Forest Floods and Agricultural Grasslands. Tartu, 2016, 124 p.
101. **Kaarel Piip.** Development of LIBS for *in-situ* study of ITER relevant materials. Tartu, 2016, 93 p.
102. **Kadri Isakar.** ^{210}Pb in Estonian air: long term study of activity concentrations and origin of radioactive lead. Tartu, 2016, 107 p.
103. **Artur Tamm.** High entropy alloys: study of structural properties and irradiation response. Tartu, 2016, 115 p.
104. **Rasmus Talviste.** Atmospheric-pressure He plasma jet: effect of dielectric tube diameter. Tartu, 2016, 107 p.
105. **Andres Tiko.** Measurement of single top quark properties with the CMS detector. Tartu, 2016, 161 p.
106. **Aire Olesk.** Hemiboreal Forest Mapping with Interferometric Synthetic Aperture Radar. Tartu, 2016, 121 p.
107. **Fred Valk.** Nitrogen emission spectrum as a measure of electric field strength in low-temperature gas discharges. Tartu, 2016, 149 p.
108. **Manoop Chenchiliyan.** Nano-structural Constraints for the Picosecond Excitation Energy Migration and Trapping in Photosynthetic Membranes of Bacteria. Tartu, 2016, 115p.
109. **Lauri Kaldamäe.** Fermion mass and spin polarisation effects in top quark pair production and the decay of the higgs boson. Tartu, 2017, 104 p.
110. **Marek Oja.** Investigation of nano-size α- and transition alumina by means of VUV and cathodoluminescence spectroscopy. Tartu, 2017, 89 p.
111. **Viktoriia Levushkina.** Energy transfer processes in the solid solutions of complex oxides. Tartu, 2017, 101 p.
112. **Mikk Antsov.** Tribomechanical properties of individual 1D nanostructures: experimental measurements supported by finite element method simulations. Tartu, 2017, 101 p.
113. **Hardi Veermäe.** Dark matter with long range vector-mediated interactions. Tartu, 2017, 137 p.

114. **Aris Auzans.** Development of computational model for nuclear energy systems analysis: natural resources optimisation and radiological impact minimization. Tartu, 2018, 138 p.
115. **Aleksandr Gurev**. Coherent fluctuating nephelometry application in laboratory practice. Tartu, 2018, 150 p.
116. **Ardi Loot**. Enhanced spontaneous parametric downconversion in plasmonic and dielectric structures. Tartu, 2018, 164 p.
117. **Andreas Valdmann.** Generation and characterization of accelerating light pulses. Tartu, 2019, 85 p.
118. **Mikk Vahtrus.** Structure-dependent mechanical properties of individual one-dimensional metal-oxide nanostructures. Tartu, 2019, 110 p.
119. **Ott Vilson.** Transformation properties and invariants in scalar-tensor theories of gravity. Tartu, 2019, 183 p.
120. **Indrek Sünter.** Design and characterisation of subsystems and software for ESTCube-1 nanosatellite. Tartu, 2019, 195 p.
121. **Marko Eltermann**. Analysis of samarium doped TiO_2 optical and multiresponse oxygen sensing capabilities. Tartu, 2019, 113 p.
122. **Kalev Erme**. The effect of catalysts in plasma oxidation of nitrogen oxides. Tartu, 2019, 114 p.